Master Thesis of Science

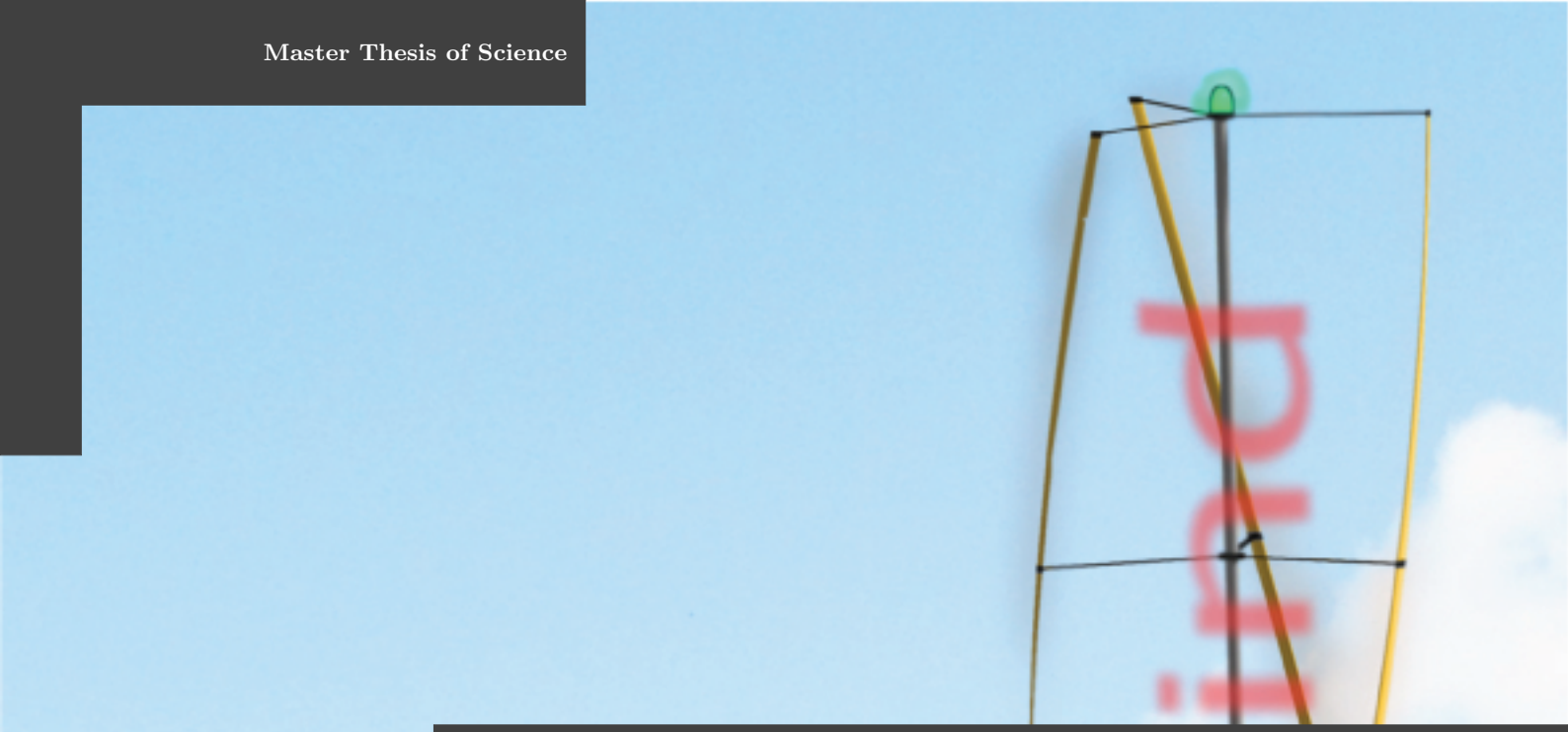

Investigation on Fault-ride Through Methods for VSC-HVDC Connected Offshore Wind Farms

Overview and New Proposal for Fault Ride Through

Wenye Sun

June 25, 2015

European Wind Energy Master - EWEM- Electric Power System Track

Investigation on Fault-ride Through Methods for VSC-HVDC Connected Offshore Wind Farms

Overview and New Proposal for Fault Ride Through

Master of Science Thesis

For obtaining the degree of Master of Science in Electrical Engineering at Delft University of Technology and in Technology-Wind Energy at Norwegian University of Science and Technology.

Wenye Sun

June 25, 2015

European Wind Energy Master - EWEM
DUWIND - Delft University of Technology
Norwegian University of Science and Technology

European Wind Energy Master - EWEM
Of
Electric Power System Track

The undersigned hereby certify that they have read and recommend to the European Wind Energy Master - EWEM for acceptance a thesis entitled **"Investigation on Fault-ride Through Methods for VSC-HVDC Connected Offshore Wind Farms"** by **Wenye Sun** in partial fulfillment of the requirements for the degree of **Master of Science**.

Dated: June 25, 2015

Supervisor: _____
Prof.dr. Pavol Bauer of TU Delft

Supervisor: _____
Dr. Olimpo Anaya-Lara of NTNU

Reader: _____
Dr. Henk Polinder of TU Delft

Reader: _____
E. (Minos) Kontos of TU Delft

Reader: _____
Raymundo Enrique Torres-Olguin of NTNU

Abstract

Recently, there has been a fast development and deployment of wind energy to meet the increasing electrical power demand and to limit the use of fossil fuels. More and more wind farms are planned far from shore because of good wind condition and less visual impact. This is so called offshore wind farm (OWF). In such a situation, high voltage direct current (HVDC) transmission is a favorable option for integrating these OWFs to the onshore grid, because HVDC, compared with high voltage alternating current (HVAC), has lower losses and higher transmission efficiency. For HVDC transmission, voltage source converter (VSC) has some advantages over current source converter (CSC), e.g. independent control of active power and reactive power, bidirectional power transfer for fixed voltage polarity.

When a fault occurs at the onshore ac grid which connects OWFs via VSC-HVDC, the active power cannot be fully transmitted to onshore grid, while OWFs still produce active power. The imbalanced power will increase the HVDC-link voltage. This increased dc voltage will lead to high electrical stress for the insulated gate bipolar transistor (IGBT) modules, capacitors as well as cables, and even damage them.

There have been different proposed methods to deal with this problem, e.g. chopper controlled resistor, wind turbine generator power setpoint adjustment, wind turbine grid side converter active current reduction, offshore voltage reduction. Chopper resistor method limits dc-link voltage by dissipating the imbalanced power . The second and third method reduce the power output from each wind turbine to limit the dc-link voltage increase. These two methods need communication between HVDC converter and each wind turbine. Offshore voltage reduction method initiates a controlled voltage drop by offshore converter to achieve a fast power reduction. All these four fault ride through (FRT) methods will be implemented in a test system and the effectiveness of these methods are evaluated with simulations made in PSCAD environment. Finally, based on the proposed methods, an enhanced FRT method is developed and its effectiveness is tested with the system. The advantages and disadvantages of different FRT methods are compared and summarized.

Acknowledgements

This report is the result of my master thesis as a student in European Wind Energy Master program. Many thanks to the people, who helped me, supported me and encouraged me during the whole period of doing my thesis.

First, I want to thank Prof. Olimpo Anaya-Lara, my supervisor from Norwegian University of Science and Technology (NTNU). He gave me this great opportunity to explore the field of VSC-HVDC technology. Thank you for your patience, guidance and encouragement.

Special gratitude to my supervisor Prof. Pavol Bauer and daily supervisor PhD-student E. (Minos) Kontos from Delft University of Technology (TUD). Although I did my master project in NTNU, their suggestions and guidance really helped me a lot.

My deepest gratitude goes to my daily supervisor Postdoc, Raymundo Enrique Torres-Olguin from NTNU. Thank you for introducing me to the world of PSCAD/EMTDC. Thank you for your encouragement when I met difficulties. Thank you for giving me so much precious advice on my thesis. Thank you for all the effort and time you spent on my thesis.

In addition, I want to thank my parents, my sister, and my brother for their endless love and support during my study abroad.

Finally, I want to express thanks to my girlfriend. She gave me so much love and encouragement. Thank you my beloved Liaosha.

Trondheim, Norway — Wenye Sun
June 25, 2015

Contents

List of Figures

List of Tables

Abbreviation

AC Alternating current

ACGSC AC grid side converter

DC Direct current

EU European Union

FRT Fault ride through

GSC Generator side converter

GTO Gate turn-off thyristor

HVAC High-voltage alternating current

HVDC High-voltage direct current

IGBT Insulate-gate bipolar gate transistors

MMC Modular multi-level converter

OWF Offshore wind farm

PI Proportional-Integral

PLL Phase locked loop

PWM Pulse-width modulation

SCIG Squirrel-cage induction generator

VSC Voltage source converter

WF Wind farm

WRIG wound rotor induction generator

Chapter 1

Introduction

1.1 Background

Due to the increment in electricity demand and the increased concern for the environmental impact of the conventional fossil fuel sources, a number of new generation technology, such as wind power, solar photovoltaic, tidal power, wave power, and biomass, have been developed. Among these renewable energy sources, wind energy is high-lighted because of its fast development in the last 25 years. The total wind power installed around the world has reached 369.557 GW at the end of 2014 [1]. Only in European Union (EU) annual installations of wind power have increased over the last 14 years, from 3.2 GW in 2000 to 11.8 GW in 2014 at a compound annual growth rate of 9.8% shown in Figure 1.1. The majority of the wind turbines have been installed onshore, but the large-scale expansion of onshore wind is limited by factors such as the land use and visual impact [2]. Therefore, offshore wind farms (OWFs) have shown a rapid development. Moreover, the offshore mean wind speed is higher than that in onshore sites and the turbulence is much lower [3]. All these factors have made offshore wind installation rise significantly through the years. Figure 1.2 shows the growth of offshore wind power from 2000, and it is projected till 2030.

OWFs are usually located far from load centers. Therefore, long transmission cables are required. Moreover, the capacity of these wind farms becomes larger and larger. For such offshore network, where large power will be transmitted over long distance, application of high-voltage alternating-current transmission (HVAC) technology may not be feasible [6]. The reason behind is that with increasing transmission distance, the reactive power flow will be higher due to line capacitances, which will result in large line losses [7]. Thus, an alternative is to use high-voltage direct-current transmission (HVDC) technology.

There are two HVDC technologies, i.e. current source converter (CSC) HVDC and voltage source converter (VSC) HVDC. CSC uses line-commutated switching de-

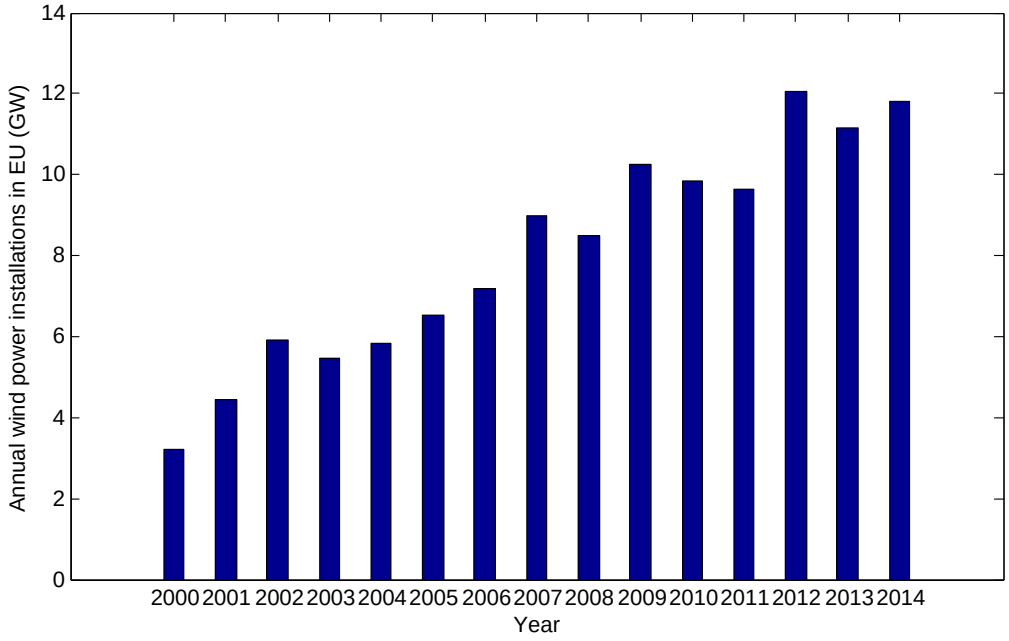

Figure 1.1: *Annual wind power installation in EU [4]*

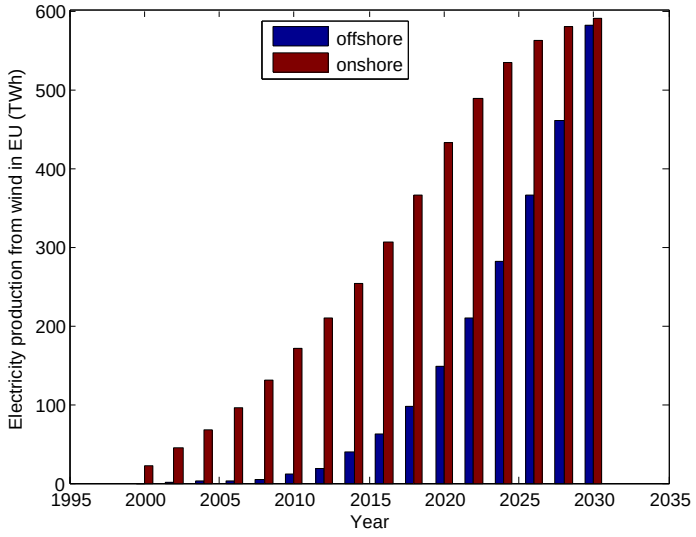

Figure 1.2: *Electricity production from wind in EU [5]*

vice, which has some limitations, for example it needs reactive power compensation devices resulting in a bulk converter station. Modern HVDC transmission systems use VSC, which is self-commutated device. This means that in VSC, the current can be made lag or lead the ac voltage, so the converter can consume or supply reactive

power to the connected ac network eliminating the reactive power compensation devices [8]. It can also make it possible to control the active power and reactive power independently. Furthermore, 1 to 2 kHz high switch frequency of pulse-width modulation (PWM) reduces the filtering requirements and power flow can be reversed without the need to reverse the dc-link voltage. All these advantages show VSC is good option for HVDC transmission.

1.2 Problem Description

When an OWF is connected to main grid through VSC-based HVDC, the HVDC voltage is controlled by the onshore HVDC converter which transfers the power to the onshore ac network. When a fault occurs at the ac grid, the onshore converter is unable to transmit all the active power to the ac grid, but OWF still inject active power to offshore converter, which will result in power imbalance between onshore converter and offshore converter shown in Figure 1.3. The resulting power imbalance will charge the capacitance in the dc-link. Without any actions, this will result in a fast increase of the dc voltage, which may damage the HVDC equipment. Therefore some strategies should be taken to regulate the power imbalance.

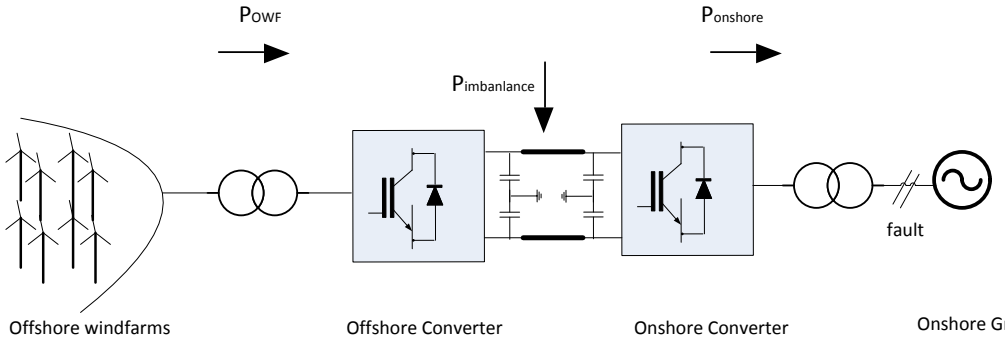

Figure 1.3: *Fault effect on power transfer for VSC-HVDC system*

This thesis investigates the possible fault ride through (FRT) methods to deal with the onshore ac fault. The model and control principle of HVDC converter and wind turbine will be first developed. Then a test system of OWF connected to main grid via HVDC will be established. After that, several FRT methods will be developed and implemented. The system will be tested under onshore short circuit conditions, to test the capability and effectiveness of the proposed FRT methods to handle these situations.

1.3 Research Objectives

The research objectives of this master project are summarized as followings:

- To implement a complete model of OWF connecting VSC-HVDC transmission system. This model includes OWF, converter transformers, VSC, dc cable, and onshore ac grid. The controller designed for wind turbine and HVDC converter is based on vector control.
- Design the controller of onshore converter based on FRT requirement of grid code.
- To implement and compare previous FRT methods proposed in literature with the established OWF connected HVDC system in this thesis. These methods include chopper resistor, wind turbine power setpoint adjustment, wind turbine active current control, and offshore voltage reduction.
- To propose a new FRT method based on the power reduction on the OWF to solve the problem of de-loading of power in OWF connected HVDC system. This new method will eliminate the need of communication between HVDC converters and wind turbine, and also improve the over-voltage control ability of VSC-HVDC system.
- Verify the capability and effectiveness of the control strategies as well as FRT methods with simulation.

1.4 Thesis Outline

This thesis contains six parts. They are organized as follows:

Chapter 1 provides an overview of the developed work.

Chapter 2 first gives a brief introduction of VSC, including the characteristic of VSC, operation principle of VSC, modeling of VSC, and PWM technique. Further, it gives a simple overview of direct control and vector control of HVDC converter. Based on vector control, the detailed design of offshore converter controller and onshore converter controller is described in the last section of this chapter.

Chapter 3 mainly explains the features and control system of wind turbines. First, it gives a basic introduction of energy conversion of wind turbine. Then, different types of generators for wind turbine and their characters are described. Finally, it presents the controller design for wind turbine, including pitch control, generator side converter (GSC) control and ac grid side converter (ACGSC) control.

Chapter 4 presents the whole system layout, comprising of OWFs and VSC-HVDC. The main components, including onshore grid, converter transformer, VSC, dc cable, OWF, and their parameters are described here. The system is tested under different wind conditions to verify it works well. The simulation tool-PSCAD/EMTDC

is introduced and some of the most important parameters in PSCAD project setting are listed in this chapter.

Chapter 5 mainly explains different FRT methods and evaluate their effectiveness through simulation in PSCAD. First Germany grid codes requirement on FRT is introduced. Then the detailed design and implementation of different FRT methods is described and their effectiveness is evaluated. Finally the advantages and disadvantages of different FRT methods are compared and summarized.

Chapter 6 draws the main conclusions from this project and gives some suggestions for future research work.

Chapter 2

Control Design for VSC-based HVDC

This chapter will first give an overview of voltage source converter (VSC) and then the control design for VSC-based HVDC is presented. It is organized as followings: Section 1 describes the characteristic and advantages of VSC. Then, section 2 gives a brief overview of the operation principle of VSC. In section 3, pulse-width modulation (PWM) technique is introduced. The model of VSC is given in section 4. Section 5 presents the general control methods for VSC, including direct control and vector control. Finally, the detailed design for VSC-HVDC controller is described in section 6.

2.1 Characteristics and Advantages of VSC

Current source converter (CSC) uses thyristors. Thyristors can only be turned on by control action, and rely on the external ac system to provide turn-off action. This limits the usefulness of HVDC in some circumstances because it means that the ac system to which the HVDC converter is connected must have synchronous machine in order to provide the commutating voltage [9].

Other types of semiconductor devices, such as insulated-gate bipolar transistor (IGBT) and gate turn-off thyristor (GTO), can be both turned on and turned off by control action. As a result, IGBT can be used to make self-commutated converters, which is also called VSC.

More and more HVDC systems adopt VSC. Compared with classical HVDC, which uses CSC, VSC based HVDC has many advantages [10].

- With PWM technology, VSC can control the magnitude and phase angle of ac side voltage. This allows VSC-HVDC system to independently control both active power and reactive power flow within the operating range of VSC-HVDC system.

- VSC-HVDC can generate leading and lagging reactive power. This capability can be used to control the ac network voltage, and thereby improve the power quality.
- Unlike HVDC classic converters, the VSC-HVDC can operate at very low power, or even zero power.
- In VSC-HVDC, the power reversal is obtained by changing the direction of dc current, not by changing the polarity of dc voltage as for HVDC classic converter. This enables VSC-HVDC transfer active power in either of the two directions with the same control setup and with the same main circuit configuration.
- By controlling the grid voltage level, VSC-HVDC can reduce the losses in the connected grid.
- VSC-HVDC can support grid restoration in the event of power disruptions, when voltage and frequency support is much needed.
- When a voltage collapse or black-out occurs, VSC-HVDC can instantaneously change to its own voltage and frequency reference and disconnect itself from the grid. Then the converter behaves like an idling static generator, and is ready to be connected to a black network to provide the first electricity to the grid.
- High switch frequency of PWM reduces the filtering requirements.
- VSC-HVDC has low environment impact. Since the converter station is enclosed in a building, the impact of transmission system on the environment is very low.

2.2 Operating Principle of VSC

Figure 2.1 shows single-phase half bridge VSC circuit. It consists of two switching devices (S_1 and S_2) with two antiparallel diodes (D_1 and D_2) to provide the return circuit for the current when bidirectional power flow is required.

The operation of this circuit is shown in Figure 2.2. Two complementary control signals for turning on and off the switches S_1 and S_2 are implemented. When the switch S_1 is turned on, the output voltage equals the voltage of C_1 which is $\frac{V_{dc}}{2}$. If the output current is positive, with respect to the direction shown in Figure 2.1, then the current flows through switch S_1. If the output current is negative, then the current flows through diode D_1. Similarly, when the switch S_2 is turned on, the output voltage equals the voltage of C_2 which is $-\frac{V_{dc}}{2}$. If the output current is positive, with respect to the direction shown in Figure 2.1, then the current flows through diode D_2. If the output current is negative, then the current flows through switch S_2.

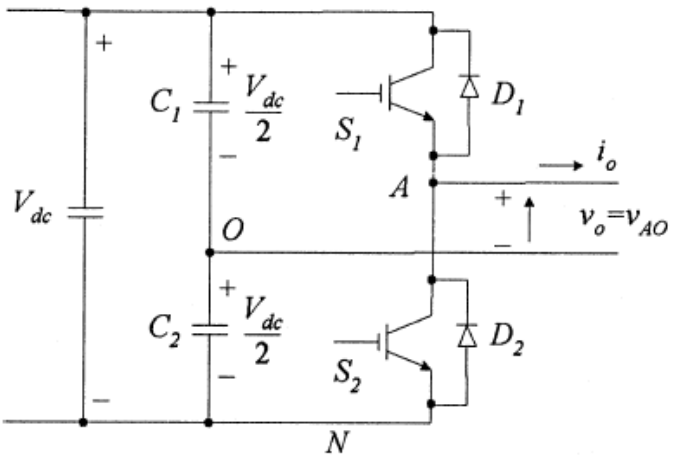

Figure 2.1: *Single phase half bridge VSC [11]*

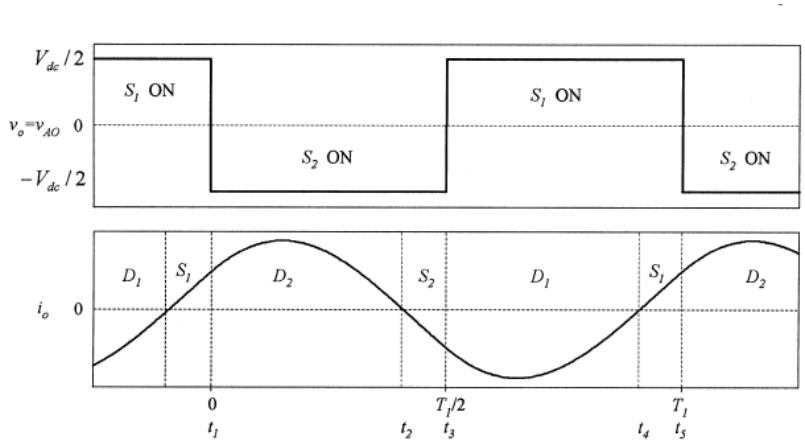

Figure 2.2: *Waveform of Single phase half bridge VSC circuit operation [11]*

There are two distinct modes of operation associated with the transfer of power from the dc to the ac side. When the power flows from the dc bus to the ac side, the converter operates as an inverter. In the case that the power is negative which means power is returned back to the dc bus from the ac side, the converter operates as a rectifier [11].

Figure 2.1 shows single-phase half bridge VSC circuit, but the work principle of three-phase six-step VSC is the same. In three-phase six-step VSC, there are six switches S_1-S_6 and six antiparallel diodes D_1-D_6 organized in three legs. The number of the switches indicates their order of being turned on. Each of the switch remains on for 180° and every 60° a new switch is turned on and the one in the same leg is turned off. For detailed operation of three-phase six-step VSC, please refer to [11].

2.3 PWM Technique

PWM technology is quite an old and proven concept and has dominated the industry since the early 1960s, especially for adjustable speed motor drives [11]. The technology is used in the VSC-HVDC solution presented by ABB under the brand HVDC-light [12].

The two level PWM method can be described with the assistance of Figure 2.3. The method is based on the comparison between a reference signal (sinusoidal) having the desired frequency f_1 and a carrier signal (triangular) with a relatively higher frequency f_c [11]. This comparison generates a modulated square-wave signal that can be used to turn on or turn off the switches of a given converter technology.

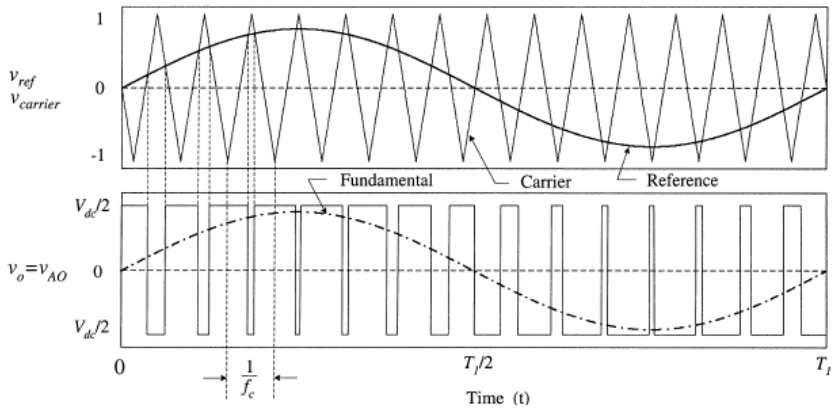

Figure 2.3: *Waveform of principle of PWM [11]*

The PWM showed in Figure 2.3 is used for one phase VSC, but the principle is the same in three phase system. The only difference is the numbers of reference signal. In a three phase six-switch VSC, since there are three legs, three reference signals (sinusoidal) phase-shift by 120° from one another compares with a carrier signal (triangular). This comparison can generate three square-wave signals to control the switches on three legs.

2.4 Model of VSC

Figure 2.4 shows the basic structure of the VSC-HVDC transmission system. V_{sabc} $(=[V_{sa}\ V_{sb}\ V_{sc}]^T)$ represents the three phase ac source voltage. i_{sabc} $(=[\ i_{sa}\ i_{sb}\ i_{sc}]^T)$ represents the three phase current. And the converter side voltage is donated by V_{cabc} $(=[V_{ca}\ V_{cb}\ V_{cc}]^T)$. R_t and L_t are the resistance and inductance of the converter transformer. R_f and L_f is the resistance and inductance of the phase reactor. Based on the Kirchhoff Voltage Law to the VSC-HVDC circuit, the dynamic equation can be derived:

$$\frac{di_{sabc}}{d_t} = -\frac{R_1}{L_1} i_{sabc} + \frac{1}{L_1}(V_{sabc} - V_{cabc}) \tag{2.1}$$

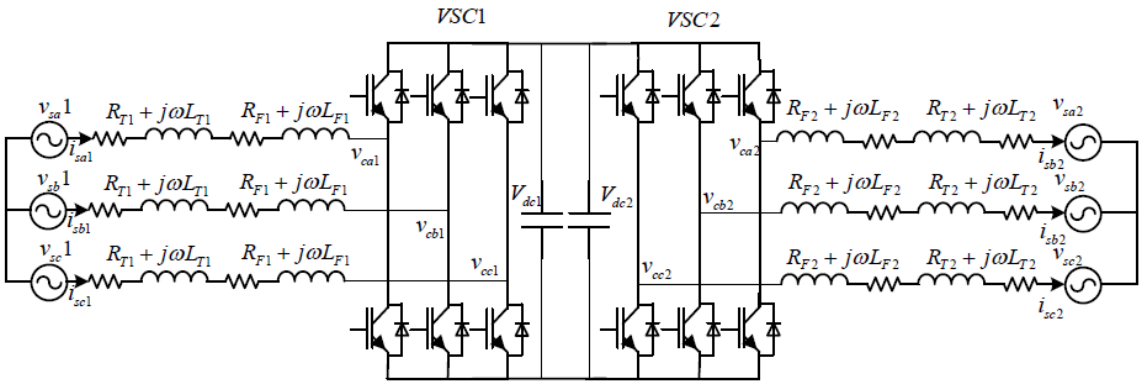

Figure 2.4: *Circuit diagram of voltage source converter connected to grid*

where $R_1 = R_{t1}+R_{f1}$ and $L_1=L_{t1}+L_{f1}$.

This model is abc coordinate representation, which is quite clear to describe the dynamic process of the system. But it is not common to use this representation for the control design of VSC because of the effort to manage a time varying three-phase model [13].

To simplify the design of control system, the three-phase quantities can be expressed in synchronous rotating dq-reference model. The idea behind this is to transfer the sinusoidal waveform to dq quantities. A key advantage is that time varying inductances in a rotating machine are constant in dq-frame [14] [15]. The transformation between abc to dq is called Park Transform and its mathematics description is shown in appendix A.

The dynamics of the VSC, in dq-frame, can be described by the following model:

$$\frac{di_{sd1}}{d_t} = -\frac{R_1}{L_1}i_{sd1} + \omega i_{sq1} + \frac{1}{L_1}(V_{sd1} - V_{cd1}) \tag{2.2}$$

$$\frac{di_{sq1}}{d_t} = -\frac{R_1}{L_1}i_{sq1} - \omega i_{sd1} + \frac{1}{L_1}(V_{sq1} - V_{cq1}) \tag{2.3}$$

where i_{sdq}, V_{sdq}, V_{cdq} represents the ac current, ac source voltage and converter side voltage in dq coordinates, ω is the angular frequency of the reference phase voltage.

2.5 General Control Methods for VSC-HVDC

Direct control and vector control are the most widely used methods for VSC-HVDC. In direct control, the instantaneous active power and reactive power is controlled directly by controlling the phase angle and amplitude of the converter output voltage. On the other hand, vector control utilizes the converter as a controllable

current source, where the injected current vector follows a reference current vector [16]. Vector control has many advantages over direct control, e.g. decoupled control of active power and reactive power, better power quality. The controller of VSC-HVDC in this thesis will be based on vector control.

2.5.1 Direct Control

Direct control method is a quite simple way of VSC control. The active power and reactive power can be controlled by directly changing phase shift and the magnitude of converter voltage, shown in the following equations:

$$p = \frac{V_1 V_2 \sin\theta}{X} \tag{2.4}$$

$$q = \frac{V_1 V_1 - V_1 V_2 \cos\theta}{X} \tag{2.5}$$

where V_1, V_2 is the voltage magnitude of grid and converter separately, θ is the phase angle between the grid and converter, X is the total inductance between the grid and converter. There are some limitations in this method. From the above equation, changing θ will affect the value of active power and reactive power, so independent control of active power and reactive power is not possible.

2.5.2 Vector Control

Vector control is a very popular technique in VSC-HVDC control system. In vector control, the three phase rotating voltage and current as shown in Figure 2.4 are transformed to dq reference frame before calculating the modulation index and the phase angle. The angle between α-axis of α,β frame and d-axis of d-q frame is used for the transformation between abc and dq frame, shown in Figure 2.5. The angular position of the voltage vector can be calculated by:

$$\theta = tan^{-1}(\frac{v_\alpha}{v_\beta}) \tag{2.6}$$

where v_α and v_β are the components of voltage in α,β reference frame [16]. The information on this instantaneous phase angle of the grid voltage is very necessary for independent control of active power and reactive power. This value can be calculated by using a Phase Locked Loop (PLL).

The control system of the VSC is composed of inner loop control and outer loop control. The main function of the inner loop control is to control the ac current towards its reference. The inner loop current controller is designed according to the decoupled equations (2.2) and (2.3). The outer loop control is used to provide a reference value for the inner loop control. Generally there are four control modes for outer loop controller: dc voltage control, ac voltage control, active power control,

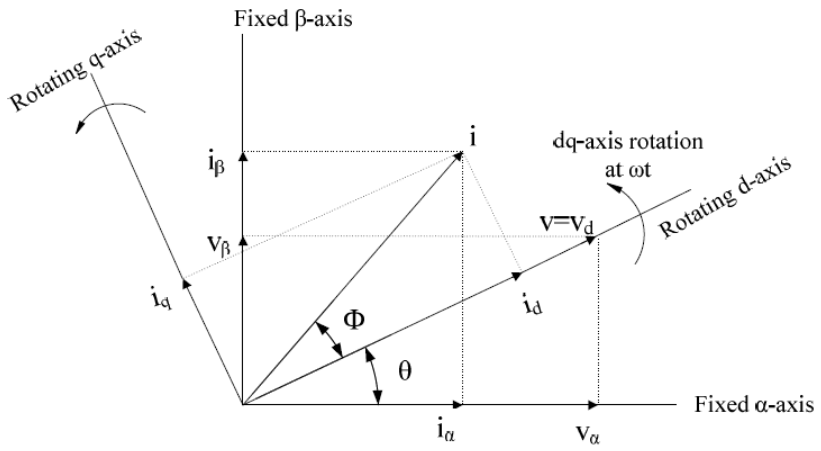

Figure 2.5: *Transformation between different coordinate system*

and reactive power control. The choice of controller to be added to VSC controller depends on the application of the VSC-HVDC. The detailed design of VSC-HVDC controller for integration of OWF is described in the next section.

2.6 Controller Design for VSC-HVDC

The control objective of VSC in VSC-HVDC system is to control the accurate transfer of active power and reactive power. In conventional ac grid, the frequency is fixed which is imposed by synchronous generators. In this case, the controller needs to determine the grid frequency and synchronize the converter to it [13]. However, when VSC-HVDC is used for integration of OWF to main grid, the offshore converter controller needs to provide a reference grid, with constant voltage magnitude and constant frequency. Then the OWF output power can be transmitted to the offshore converter. For the onshore converter, it is used to regulate the dc voltage, and provide reactive power compensation to support voltage recovery when onshore fault occurs. This section mainly focuses on the VSC controllers design which is used for integration OWF to onshore grid. It includes the controller of offshore converter which connects the OWF and the controller of onshore converter which connects the main ac grid.

This section is organized as follows: First, based on vector control, a model based offshore converter controller is designed in detail. Then, based on grid low voltage ride through requirement, the onshore converter controller is designed with a feedforward block to provide reactive power compensation when fault occurs.

2.6.1 Offshore Converter Controller Design

When VSC-HVDC connects to OWF, because the wind turbines can control active power and reactive power by themselves, the basic function of the offshore converter

controller is to maintain the ac voltage and frequency in the OWF grid. In other words, the offshore converter behaves like an infinite bus bar, all the power produced by the OWF can be absorbed automatically and transmitted to the onshore main grid.

To realize this control objective, there are different methods. One simple way is to control the ac voltage magnitude directly, as described in [17]. The offshore converter is controlled and operated as a voltage source with constant frequency (f) and angle (θ). The only feedback control loop used is the ac voltage loop, which controls the voltage magnitude of offshore converter via modulation index M. The diagram of the controller is shown in Figure 2.6.

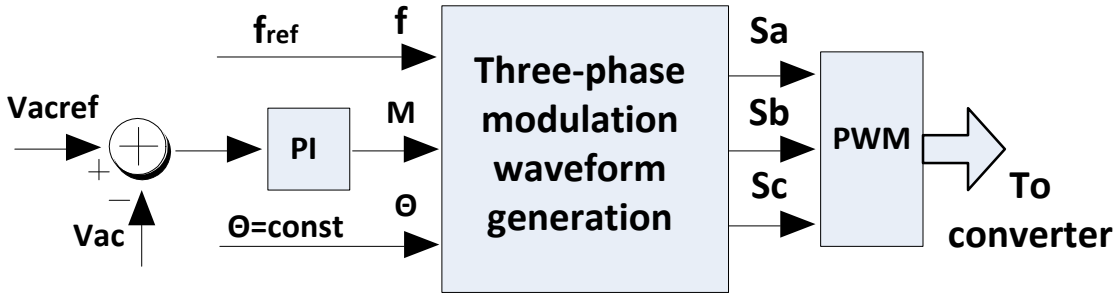

Figure 2.6: *Block diagram of ac voltage controller for offshore converter*

However it has some limitations [13]:

- There is no current loop control, so it is difficult to limit the current in the converter.
- The controller parameters have great influence on the behavior of offshore converter because the control design is not based on the model. If the controller is not tuned well, there will be some transient and dynamic in the system. As a result, it is difficult in synchronizing the OWF grid with the voltage produced by offshore converter.

In order to overcome these limitations, this thesis uses model based control including inner loop control and outer loop control. The objective of inner loop is to control the current. The objective of outer loop is to control the ac voltage and provide the current reference for the inner loop. This controller can be modeled in the synchronously rotating reference frame and PI controller can be used here.

The circuit diagram of OWF connected to offshore converter is shown in Figure 2.7, which is used to design the model based controller for offshore converter.

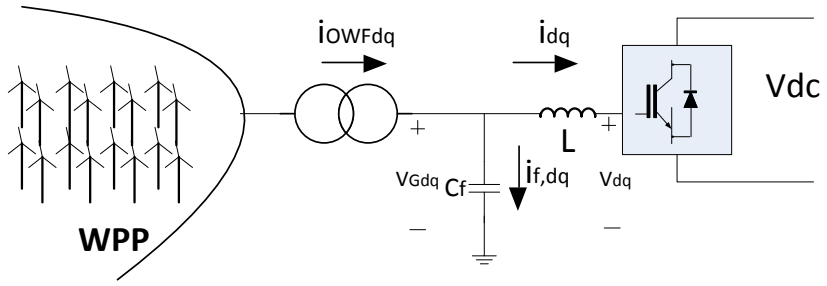

Figure 2.7: *Circuit diagram of offshore wind farm connected to offshore converter*

Applying Kirchhoff voltage law and current law to the circuit shown in Figure 2.7 in dq-coordinates:

$$C_f \frac{d}{dt} v_{Gd} = i_{OWFd} - id + \omega C_f v_{Gq} \tag{2.7}$$

$$C_f \frac{d}{dt} v_{Gq} = i_{OWFq} - iq - \omega C_f v_{Gd} \tag{2.8}$$

$$L \frac{d}{dt} i_d = v_{Gd} - v_d + \omega L i_q \tag{2.9}$$

$$L \frac{d}{dt} i_q = v_{Gq} - v_q - \omega L i_d \tag{2.10}$$

where v_{Gd} and v_{Gq} represent the voltage of the OWF grid, i_{OWFd} and i_{OWFq} represent the current flowing from OWF, i_d and i_q represent the current flowing into the converter. v_d and v_q represent the voltage at the input of VSC. ω is the frequency of the offshore grid. C_f and L represent the filter capacitance and coupling inductance separately shown in Figure 2.7. All the value above is in dq-coordinates.

As described before, the inner loop control and outer loop control is considered here. For inner loop, based on equation 2.9 and 2.10, the error between the reference current i^*_{dq} and the measured current flow into offshore converter through a Proportional-Integral (PI) to produce the reference voltage for the input of converter, shown in the equation below:

$$v^*_d = v_{Gd} + \omega L i_q - k_{p1}(i^*_d - i_d) - k_{i1} \int (i^*_d - i_d) \tag{2.11}$$

$$v_q^* = v_{Gq} - \omega L i_d - k_{p1}(i_q^* - i_q) - k_{i1}\int (i_q^* - i_q) \tag{2.12}$$

where k_{p1} and k_{i1} are the parameters of PI regulator.

The outer loop generates the immediate current reference i_{dq}^*. Based on equation 2.7 and 2.8, the error between the reference voltage v_{Gdq}^* and the measured offshore grid voltage can be used to produce the current reference through a PI controller. The equation is given below:

$$i_d^* = i_{OWFd} + \omega C_f v_{Gq} - k_{p2}(v_{Gd}^* - v_{Gd}) - k_{i2}\int (v_{Gd}^* - v_{Gd}) \tag{2.13}$$

$$i_q^* = i_{OWFq} - \omega C_f v_{Gd} - k_{p2}(v_{Gq}^* - v_{Gq}) - k_{i2}\int (v_{Gq}^* - v_{Gq}) \tag{2.14}$$

where k_{p2} and k_{i2} are the parameters of PI regulator.

For more detailed design of inner loop controller and outer loop controller can refer to [13]. Based on equation (2.11), (2.12), (2.13) and (2.14), the control diagram of offshore converter is shown in Figure 2.8.

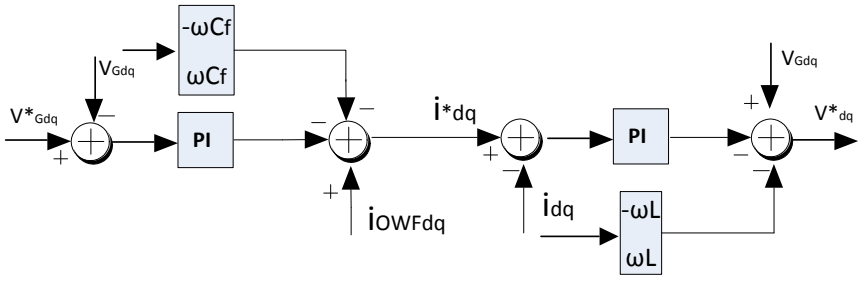

Figure 2.8: *Control diagram of offshore converter controller*

2.6.2 Onshore Converter Controller Design

In normal operating conditions, the control objective of onshore converter is to regulate the dc-link voltage which enables transfer the power from OWF to the onshore grid. During onshore grid dips, the onshore converter should regulate the reactive power to provide voltage support.

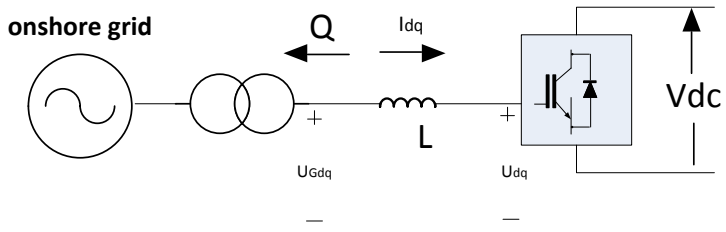

Figure 2.9: *Circuit diagram of onshore converter connected to onshore grid*

The circuit diagram of onshore converter connected to onshore grid is shown in Figure 2.9 , which is used to design the cascade controller for onshore converter.

In order to design the control system for onshore converter, the dynamic model of converter connecting onshore grid in synchronous reference frame has been developed as:

$$U_d = U_{G_d} + \omega L I_q - L\frac{d}{dt}I_d \tag{2.15}$$

$$U_q = U_{G_q} - \omega L I_d - L\frac{d}{dt}I_q \tag{2.16}$$

where U_d and U_q are the voltage at the input of the converter, U_{G_d} and U_{G_q} are the onshore grid voltage, I_d and I_q represent the currents flowing into the converter, L represents the inductance of the phase reactor, ω is the frequency of the onshore grid.

To facilitate the design of controller, d-axis has been aligned with the onshore ac voltage and q-axis is 90° ahead of d-axis, as shown in Figure 2.5. With this choice, U_{G_d}=U_G and U_{G_q}=0, which makes design of control easier. The same with the controller of offshore converter, a cascade controller is used here.

The block diagram of the controller is shown in Figure 2.10 . The inner loop controller is similar with that of offshore converter. A PI is adopted and the governing equation to produce the voltage reference for the converter (U_d^*, U_q^*) in the inner current loop, which is given by:

$$U_d^* = U_{G_d} + \omega L I_q - k_{p3}(I_d^* - I_d) - k_{i3}\int (I_d^* - I_d) \tag{2.17}$$

$$U_q^* = U_{G_q} - \omega L I_d - k_{p3}(I_q^* - I_q) - k_{i3}\int (I_q^* - I_q) \tag{2.18}$$

where k_{p3} and k_{i3} are the parameters for PI controller.

The outer loop controller regulates the dc voltage of HVDC-link and the reactive power flow to the grid. As mentioned above, d-axis is aligned with the grid voltage in synchronous reference frame. Then U_{G_d} equals U_G, U_{G_q} equals 0 which allows the control of active power and reactive power decoupled. Hence, the reference for d-axis control will regulate the active power flow, here is the dc voltage. In other words, the difference between the reference dc voltage and the voltage measured at the dc-link will be applied to a PI controller and the output will be used as the reference of I_d. In a similar way, the reference for q-axis will control the reactive power flow and the difference between reference reactive power and measured reactive power will be used to produce the reference of I_q. As is shown in the following equation:

$$I_d^* = k_{p4}(V_{dc}^* - V_{dc}) + k_{i4}\int (V_{dc}^* - V_{dc}) \tag{2.19}$$

$$I_q^* = k_{p5}(Q^* - Q) + k_{i5}\int (Q^* - Q) \tag{2.20}$$

where k_{p4},k_{p5} and k_{i4},k_{i5} are the parameters for PI controller.

Just as mentioned before, onshore converter should provide reactive power compensation during onshore grid voltage dips. It is achieved by adding a feed-forward block of LVRT in Figure 2.10, with the deadzone-linear function [18]:

$$\Delta I_q = K_r sign(\Delta U_{grid}) max\{|\Delta U_{grid}| - \Delta V_{thres}, 0\} \tag{2.21}$$

where,

ΔU_{grid} is the voltage difference between the reference grid voltage and measured grid voltage.

K_r is a constant, based on German grid code, its value is 2.

V_{thres} is voltage dead band, and its value is 5%.

The magnitude of the current output is limited with respect to the thermal limits of power electronics devices. In steady state, the active current component has the priority. But in case of grid fault, the reactive current component takes precedence over the active component to provide voltage support for the grid.

2.7 Summary

This chapter gave a brief overview of VSC, including the characteristics of VSC, operating principle of VSC, PWM technique, modeling of VSC, and general control

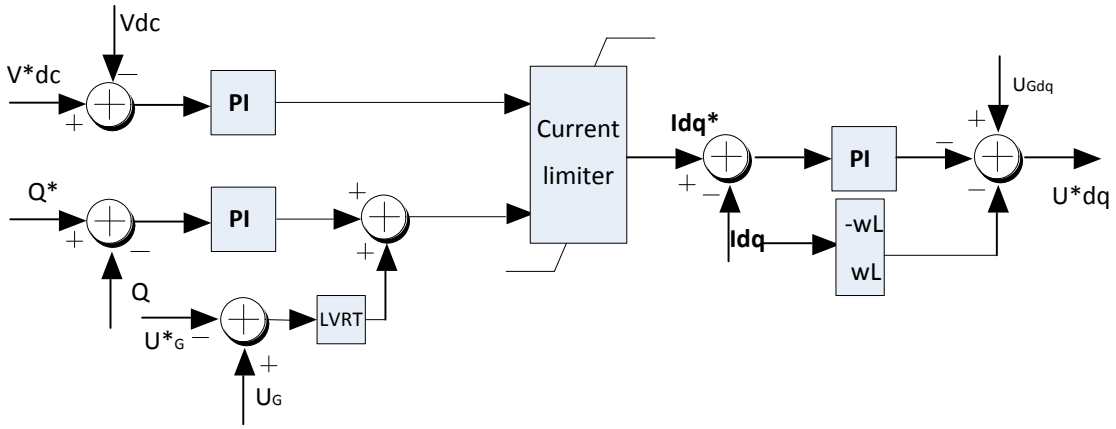

Figure 2.10: *Circuit diagram of onshore converter controller*

methods of VSC. It also presented the detailed controller design for offshore converter and onshore converter. The offshore converter is used to maintain a constant voltage for OWF grid and the onshore converter is used to regulate the dc voltage in HVDC-link and provide reactive power compensation during fault. In the next chapter, wind turbine and its control will be described.

Chapter 3

Wind Turbine and its Control

Since the first concepts of wind turbines used for electricity production were built at USA and Denmark around 1890, wind turbines have developed more than one hundred years. Within the recent one hundred years, the size of wind turbines become larger and larger, from KWs to MWs. Besides, different kinds of generator types have been developed, e.g. fixed speed generator, limited variable speed generator, and variable speed generator. Most of these wind turbines are installed onshore, but because of better wind condition and extensive space, OWFs show a rapid development in recent years and they will also develop fast in the future.

This chapter will first describe the energy conversion with a rotor. Then, it will present different kinds of generators for wind turbines and their characteristics. Finally, the controller design of wind turbine including pitch control and back-to-back converter control will be explained in the last section.

3.1 Power Capture of Wind Turbine

The kinetic energy of the air through the rotor blade is described by:

$$Ke = \frac{1}{2}\rho V v^2 \tag{3.1}$$

where ρ is the air density, V is the volume of the air, and v is the velocity of the air. V can also be expressed as:

$$V = Av \tag{3.2}$$

where A is the area swept by the wind turbine.

So the theoretical power obtained from a wind turbine is

$$P_{wind} = \frac{1}{2}\rho A v^3 \tag{3.3}$$

In practice, the power is smaller because the wind speed behind the hub is not zero [19]. The real power can be extracted by the turbine, in this case a three-bladed horizontal-axis wind turbine is:

$$P_m = P_{wind} Cp(\lambda, \beta) = \frac{1}{2} Cp \rho A v^3 \tag{3.4}$$

where Cp is the power coefficient. Cp is a function of pitch angle β and tip speed ratio λ. Tip speed ratio λ is defined as the ratio of rotor blade tip speed and wind velocity, as shown below:

$$\lambda = \frac{\omega R}{v} \tag{3.5}$$

where R is the turbine radius, ω is the rotational speed of the blade.

There are several methods to determine Cp, such as blade element theory, look up tables and analytical approximation [20]. In this thesis, analytical approximation method will be used to calculate Cp with known pitch angle β and tip speed ratio λ, as shown below:

$$Cp(\lambda, \beta) = 0.5(\frac{116}{\lambda_i} - 0.4\beta - 5)e^{\frac{-18.5}{\lambda_i}} \tag{3.6}$$

$$\lambda_i = (\frac{1}{\lambda + 0.08\beta} - \frac{0.035}{\beta^3 + 1})^{-1} \tag{3.7}$$

Based on equation (3.6) and (3.7), Cp against λ and β is drawn as Figure 3.1. It shows that with a given β, the optimum Cp can be achieved by changing the value of λ.

3.2 Wind Turbine Generators

Referring to the rotational speed, wind turbine generator concepts can be classified into fixed speed, limited variable speed, and variable speed. For variable wind turbine generator, based on the rating of power converter related to generator capacity, they can be further clarified into wind generator systems with partial scale and wind generator systems with full scale power converters [21]. In summary, there are four basic wind turbine generator concepts: fixed speed, limited variable speed, variable speed with partial scale power converter, and variable speed with full scale power converter. A brief description of these concepts is given below.

3.2.1 Fixed Speed Wind Turbine Generator

The fixed speed wind turbine generator system uses a multi-stage gearbox and squirrel-cage induction generator (SCIG), directly connecting the grid through a transformer as shown in Figure 3.2. Since SCIG always draw reactive power from the grid, a capacitor is used for reactive power compensation. The advantages of

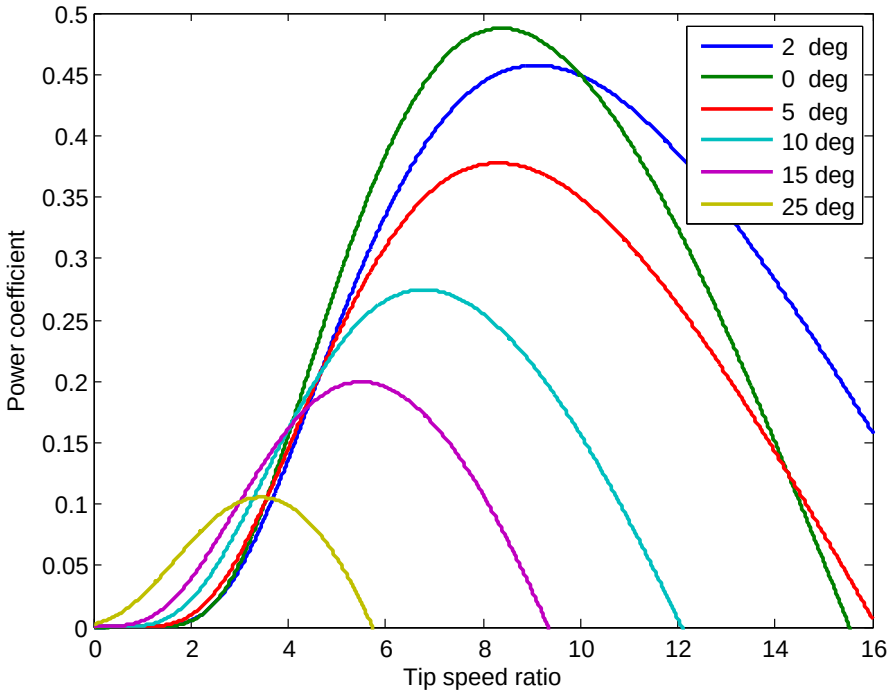

Figure 3.1: *Power coefficient as a function of pitch angle and tip speed ratio*

this wind turbine concept are its very simple setup, reliable SCIG, and relatively cheap for mass production. However, because the speed is fixed, the wind speed fluctuation will produce electromechanical torque variation, which will cause high mechanical stress on the system. Besides, multi-stage will increase the investment cost and maintenance cost. Stall control, pitch control, and active stall control are used in such wind turbines [21] [22].

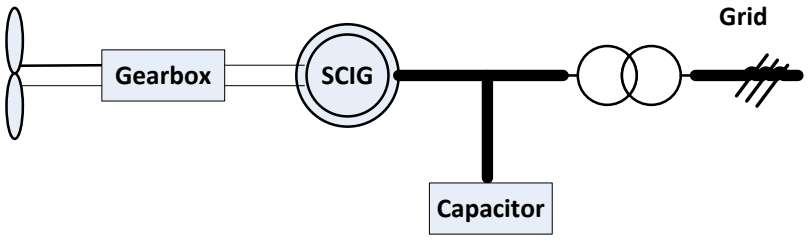

Figure 3.2: *Fixed speed wind turbine generator*

3.2.2 Limited Speed Wind Turbine Generator

The limited speed wind turbine generator is also called Optislip concept [23]. Optislip uses multi-stage gearbox and wound rotor induction generator (WRIG) as

shown in Figure 3.3. With WRIG, the slip or the rotational speed can be altered by changing the inner resistance R in the generator. A typical limited variable speed range is less than 10% above the synchronous speed [24] [25]. The same with fixed speed concept, Optislip also needs reactive power compensation. Pitch control is used in this concept.

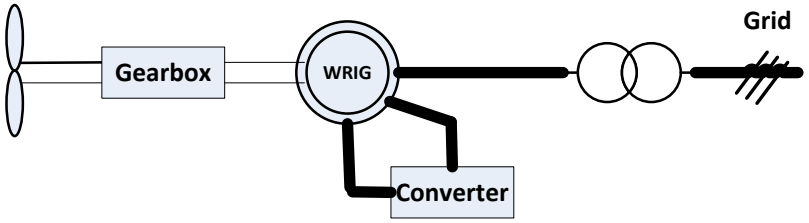

Figure 3.3: *Limited speed wind turbine generator*

3.2.3 Variable Speed Wind Turbine with Partial Scale Power Converter

This concept is also known as double fed induction generator (DFIG) concept, which uses an induction generator with a multiphase wound rotor and a partial scale power converter, as shown in Figure 3.4. The power converter controls the rotor frequency and the rotor speed [21]. As a result, this turbine can operate with variable speed of 30% around the synchronous speed. The rating of the converter is about 30% of the rated generator power [21] [24] [25]. This concept can perform reactive power compensation, and thus provide voltage support to the grid. However, the stator is directly connected to the grid, which causes problems of IGBTs during fault.

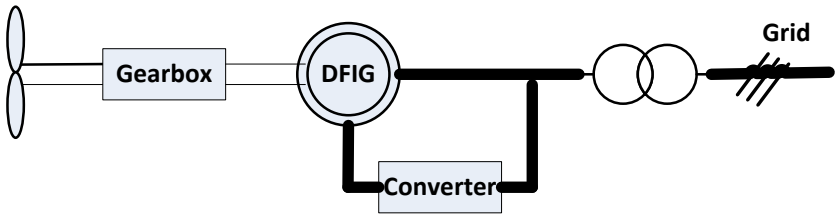

Figure 3.4: *Variable speed with partial scale power converter*

3.2.4 Variable Speed Wind Turbine with Full Scale Power Converter

The variable speed with full scale power converter turbine usually uses direct-drive generator connecting to the grid through a full back-to-back converter. With full scale power converter, this turbine can perform reactive power compensation. In addition, direct-drive generator has simplified drive train, high overall efficiency,

and high reliability by omitting the gearbox. One type of the direct-drive generator used in the market is permanent magnet synchronous generator (PMSG). The configuration of PMSG turbine is shown in Figure 3.5. PMSG does not need to provide additional power for the magnet field excitation, and thus the efficiency is improved. Besides, the absence of slip rings makes PMSG higher reliability. Recently, because the cost of PMSG is decreasing and the performance is improving, PMSG has become more and more attractive. The configuration of PMSG with full scale converter is selected in this thesis.

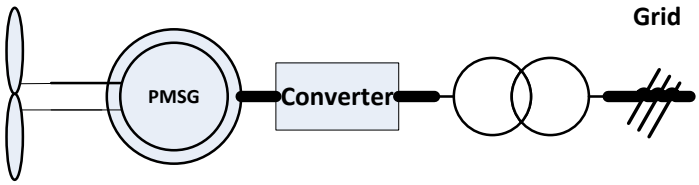

Figure 3.5: *Variable speed with full scale power converter*

3.3 Wind Turbine Control System Design

This section will introduce the controller design of wind turbine. The control system ensures wind turbines operate within the design range, for example it can keep the rotation speed within a certain range, yaw the wind turbine, start and stop wind turbine [23]. In summary, three operation modes can be identified shown in Figure 3.6.

- Region 1, for wind speed lower than the cut-in speed and higher than the cut-out speed, the power output is zero, and the turbine is in the parking mode. In this mode, the control system of wind turbine is mainly responsible for starting and stopping wind turbines.
- Region 2, for wind speed between the cut-in speed and nominal speed, the blade is pitched to the optimal θ. The rotational speed ω is controlled by the generator to keep tip speed ratio λ at its optimum value. The wind turbine is mainly operated at the electrical control interval. In this region, the electrical system can ensure a smooth power output and optimize the power output.
- Region3, for the wind speed between nominal speed and cut-out speed, two mechanical control methods are commonly used in order to limit the power output at rated value: stall regulation and pitch regulation.

This thesis mainly focus on the mechanical control design to limit the power output and electrical control design to optimize the power output. The detailed control design is given below.

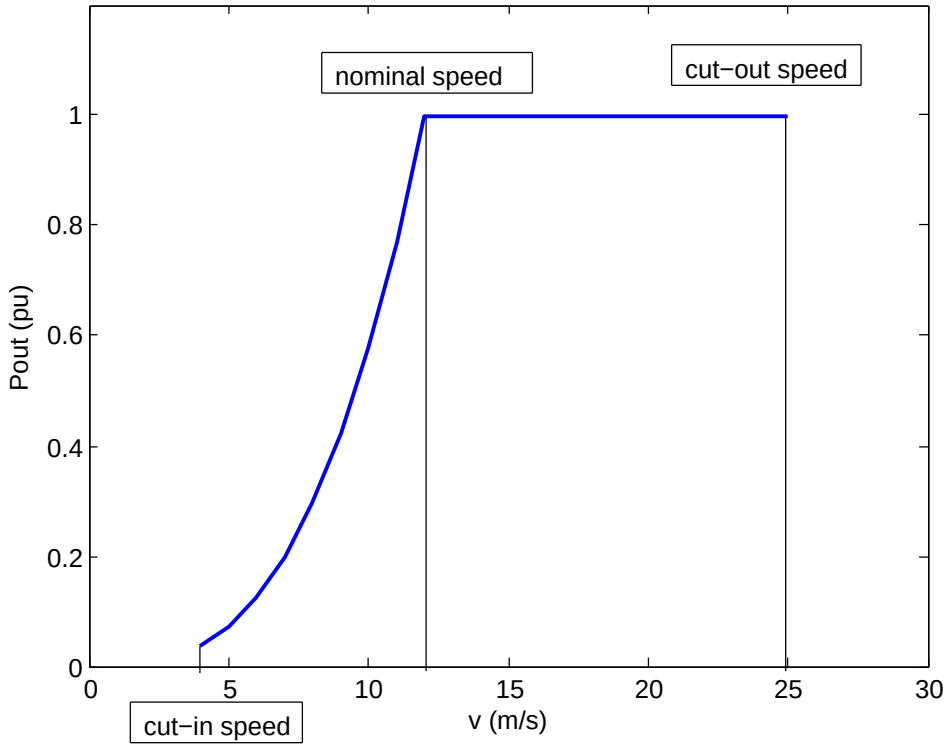

Figure 3.6: *Power curve vs wind speed*

3.3.1 Mechanical Control Design for Wind Turbine

Stall regulation is the most simple one, since the blade is fixed to the hub and cannot be pitched. The angle of attack of stall regulation wind turbine increase as wind speed increases, and thus limit the power output of wind turbines. This control strategy is usually used for fixed speed wind turbines.

Based on the equation (3.6) and (3.7), Cp is related to the blade pitch angle. On a pitch regulated machine, it is possible to actively pitch the entire blade, and hence limit the power output. Variable speed wind turbines adopt pitch control strategy. Such control can also assist start-up and emergency stop. This thesis uses pitch control.

Adjusting pitch angle of blade can provide an effective mean of limiting turbine power in strong wind speeds. One conventional pitch control is based on Proportional-Integral (PI) controller to produce the pitch angle reference. Many values can be used as the input for PI controller, e.g. wind speed, generator rotor speed, generator power [26]. This thesis uses the value of generator power to control the pitch angle, shown in Figure 3.7.

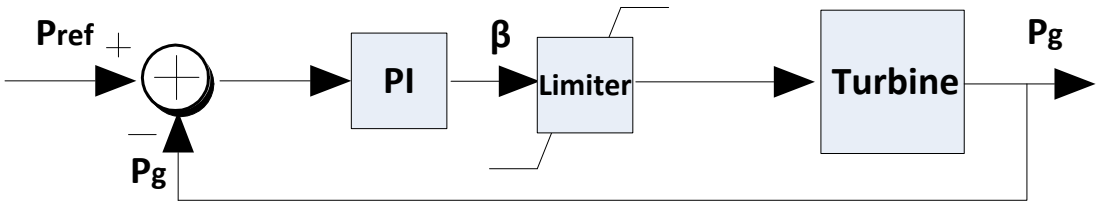

Figure 3.7: *Pitch controller for wind turbine*

The error signal between the rated power and measured generator power can be sent to a PI controller to produce the reference value of pitch angle. The controller parameters are determined with trial and error methods. A limiter is applied to limit the pitch rate within 8°/s, which is used to avoid excessive loads during normal regulation procedure.

The conventional PI controller for pitch adjustment is a simple and effective method. But when the system has strong dynamics or they contain significant non-linearity, fuzzy logic controller can be adopted, see [26] for more information.

3.3.2 Electrical Control Design for Wind Turbine

The electrical controller design of wind turbine can be divided into two parts: generator side converter (GSC) control and ac grid side converter (ACGSC) control. GSC is used to control the rotor speed to produce maximum power and ACGSC is used to regulate the dc voltage of the back-to-back converter. How the two controllers designed are given below.

Generator Side Converter Control

The control objective for GSC is to extract the maximum power from the wind turbine. From Figure 3.8, it can be seen that for given rotational speed, for each wind speed, there is a maximum power point. These maximum power points can form an optimum power line. The task of the GSC is to track the optimum power line[13].

The interaction between the PMSG and the converter will be examined. Figure 3.9 shows the block diagram of PMSG and back-to-back converter.

In order to design the control system for GSC, the dynamic model of PMSG should be developed. To make it easier to define the controller, the equations of the

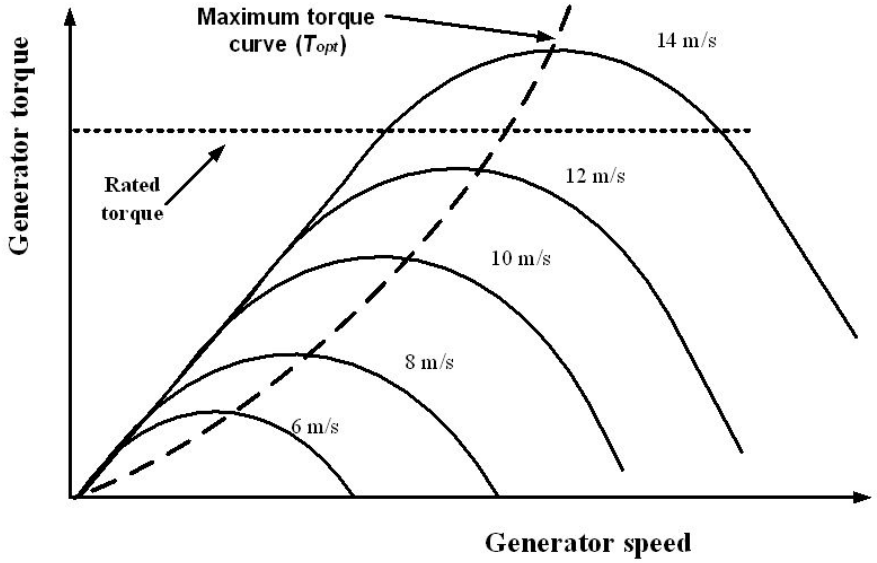

Figure 3.8: *Maximum output power vs generator rotational speed*

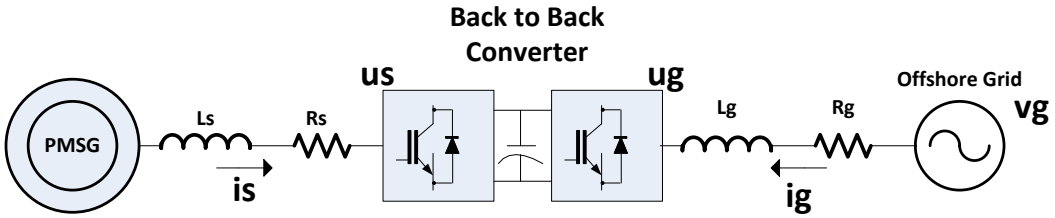

Figure 3.9: *Circuit diagram of full rated converter wind turbine with PMSG*

generator are projected on a reference coordinate system rotating synchronously with the magnet flux [27]. In other words, the rotor flux is aligned with d-axis, then q-axis is 90 ahead of d-axis. Then the dynamic model of PMSG is given by:

$$u_{sd} = -R_s i_{sd} - L_s \frac{di_{sd}}{d_t} + L_s \omega i_{sq} \tag{3.8}$$

$$u_{sq} = -R_s i_{sq} - L_s \frac{di_{sq}}{d_t} - L_s \omega i_{sd} + \omega \psi \tag{3.9}$$

where i_{sd} and i_{sq} are the stator current, u_{sd} and u_{sq} represent the stator voltage, R_s and L_s are the generator resistance and inductance respectively, ω is the generator speed and ψ is the magnet flux.

Based on equation (3.8) and (3.9), cascade control can be used here: inner loop and outer loop. For inner loop, the PI can act upon the current deviation from

the reference current signal(i^*_{sd}, i^*_{sq}) and measured current(i_{sd},i_{sq}) to produce the voltage reference for the converter (u^*_{sd}, u^*_{sq}), as given below [28]:

$$u^*_{sd} = \omega L_s i_{sq} + k_{p6}(i^*_{sd} - i_{sd}) + k_{i6}\int (i^*_{sd} - i_{sd}) \tag{3.10}$$

$$u^*_{sq} = \omega\psi - \omega L_s i_{sd} + k_{p6}(i^*_{sq} - i_{sq}) + k_{i6}\int (i^*_{sq} - i_{sq}) \tag{3.11}$$

where k_{p6} and k_{i6} are the parameters for PI controller.

The outer loop regulates the active power. As mentioned before, the control objective of GSC is to extract the maximum power from the wind turbine. So the power from the generator is measured and compared to the reference power. The difference will be applied to a PI controller and the output will be used as the reference of i_q, as is shown in the following equation:

$$i^*_{sq} = k_{p7}(P^* - P) + k_{i7}\int (P^* - P) \tag{3.12}$$

where k_{p7} and k_{i7} are the parameters for PI controller.

The i_{sd} set-point, i^*_{sd} is set to zero here to minimize the stator current, and hence to minimize the resistive losses in the stator.

Notice that the reference power P^* is obtained using the optimum power line shown in Figure 3.8. The block diagram of the overall controller is depicted in Figure 3.10.

AC Grid Side Converter Control

The control objective of ACGSC is to maintain the dc-link voltage and control the reactive power. In order to design the control system for the grid side converter, the dynamic model of converter connecting offshore grid in synchronous reference frame has been developed as:

$$u_{gd} = v_{gd} - i_{gd}R_g - L_g\frac{d}{dt}i_{gd} + \omega L_g i_{gq} \tag{3.13}$$

$$u_{gq} = v_{gq} - i_{gq}R_g - L_g\frac{d}{dt}i_{gq} - \omega L_g i_{gd} \tag{3.14}$$

where u_{gd} and u_{gq} are the voltage at the input of the converter, v_{gd} and v_{gq} are the offshore grid voltage, i_{gd} and i_{gq} represent the currents flowing into the converter, L_g and R_g represent the inductance and resistance coupling the converter and offshore grid, ω is the frequency of the offshore grid.

To facilitate the design of controller, d-axis has been aligned with the offshore ac voltage and q-axis is 90° ahead of d-axis. With this choice, Then v_{gd}=v_g and v_{gq}=0,

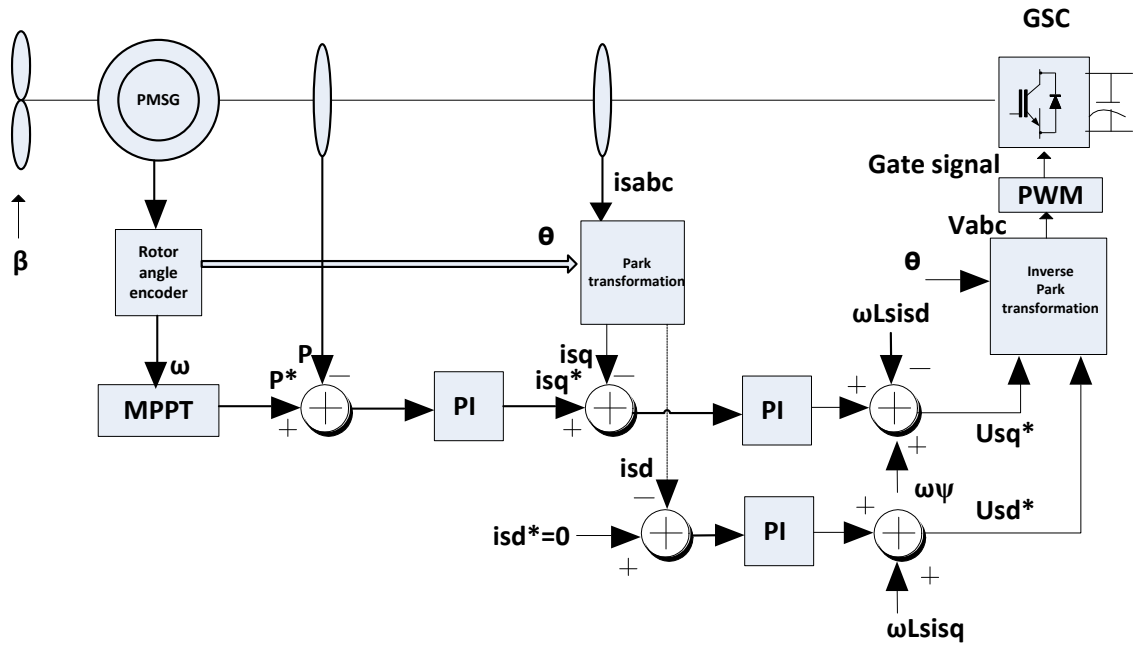

Figure 3.10: *Circuit diagram of generator side converter control*

which makes design of control easier. The same with GSC, a cascade controller is used here.

The block diagram of the controller is shown in Figure 3.11 . The inner loop control is similar with the controller of GSC. A PI controller is adopted and the governing equation to produce the voltage reference for the converter (u^*_{gd}, u^*_{gq}) in the inner current loop, which is given by:

$$u^*_{gd} = v_{gd} + \omega L_g i_{gq} - k_{p8}(i^*_{gd} - i_{gd}) - k_{i8}\int (i^*_{gd} - i_{gd}) \tag{3.15}$$

$$u^*_{gq} = v_{gq} - \omega L_g i_{gd} - k_{p8}(i^*_{gq} - i_{gq}) - k_{i8}\int (i^*_{gq} - i_{gq}) \tag{3.16}$$

where k_{p8} and k_{i8} are the parameters for PI controller.

The outer loop controller regulates the dc voltage of the back-to-back converter and the reactive power flowing to the grid. As mentioned above, d-axis is aligned with the offshore grid voltage in synchronous reference frame, and then v_{gd}=v_g and v_{gq}=0. The difference between the reference dc voltage and the voltage measured at the dc-link will be applied to a PI controller and the output will be used as the reference of I_d. In a similar way, the reference for q-axis will control the reactive power flow

and the difference between reference reactive power and measured reactive power will be used to produce the reference of I_q. As is shown in the following equation:

$$i_{gd}^{*} = k_{p9}(V_{dc}^{*} - V_{dc}) + k_{i9}\int (V_{dc}^{*} - V_{dc}) \tag{3.17}$$

$$i_{gq}^{*} = k_{p10}(Q_{ac}^{*} - Q_{ac}) + k_{i10}\int (Q_{ac}^{*} - Q_{ac}) \tag{3.18}$$

where k_{p9},k_{p10} and k_{i9},k_{i10} are the parameters for PI controller.

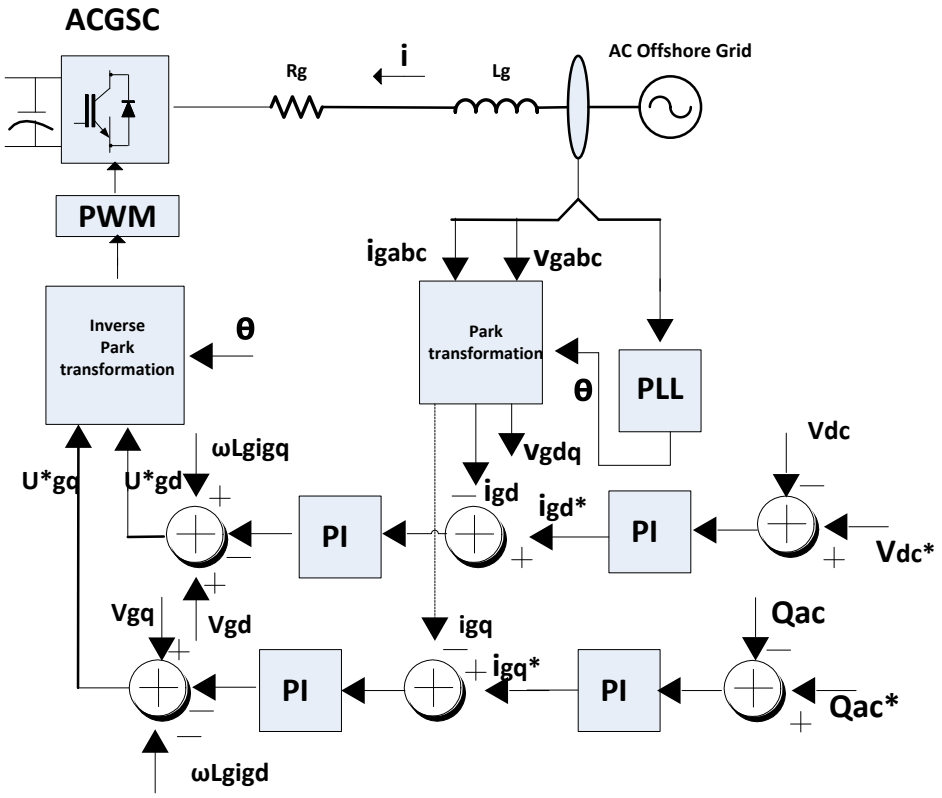

Figure 3.11: *Circuit diagram of ac grid side converter control*

3.4 Summary

Wind turbine has been briefly introduced in this chapter. The energy conversion of wind turbine and different kinds of generators for wind turbine have been described. It also gave detailed design of pitch controller, GSC controller and ACGSC controller. The pitch controller is used to limit the output power in rated value.

GSC controller is used to track the maximum power from wind turbine. ACGSC controller regulates the dc voltage between the back-to-back converter and also the reactive power. In next chapter, a test system will be presented and test under different wind conditions.

Chapter 4

System Layout and Operation of OWF connected HVDC system

This chapter shows the whole system layout including wind turbines and VSC-HVDC, which will be used as the test system. Different components and their parameters are discussed in this chapter. Then the start-up sequence of the system is described. Next, the most important parameters in PSCAD project setting are listed. Finally, the system is tested on steady state to demonstrate that it works well and is suitable for simulation study of fault.

4.1 Main Circuit Components and Parameters

Two OWFs with capacity of 200MW and 300MW connected to the onshore grid via VSC-HVDC is considered as the test system. The main components are onshore grid, converter transformers, VSC, dc cable, and OWFs, which are shown in Figure 4.1. These components and how their parameters derived are described in this section.

4.1.1 Onshore Grid

The onshore grid is represented by voltage source with series impedance. The grid impedance is estimated by the active power from OWFs , grid voltage level and short circuit ratio at the point of grid connection, shown in equation (4.1) . The resistance and reactance can be calculated with the grid angle, shown in equation (4.2), (4.3), (4.4). Based on Danish grid code [28], short circuit ratio of 10, grid angle of 84.3 is assumed in this thesis.

$$Z_{grid} = \frac{V_{grid}^2}{P_n S_k} = \frac{400^2}{500 * 10} = 32\Omega \tag{4.1}$$

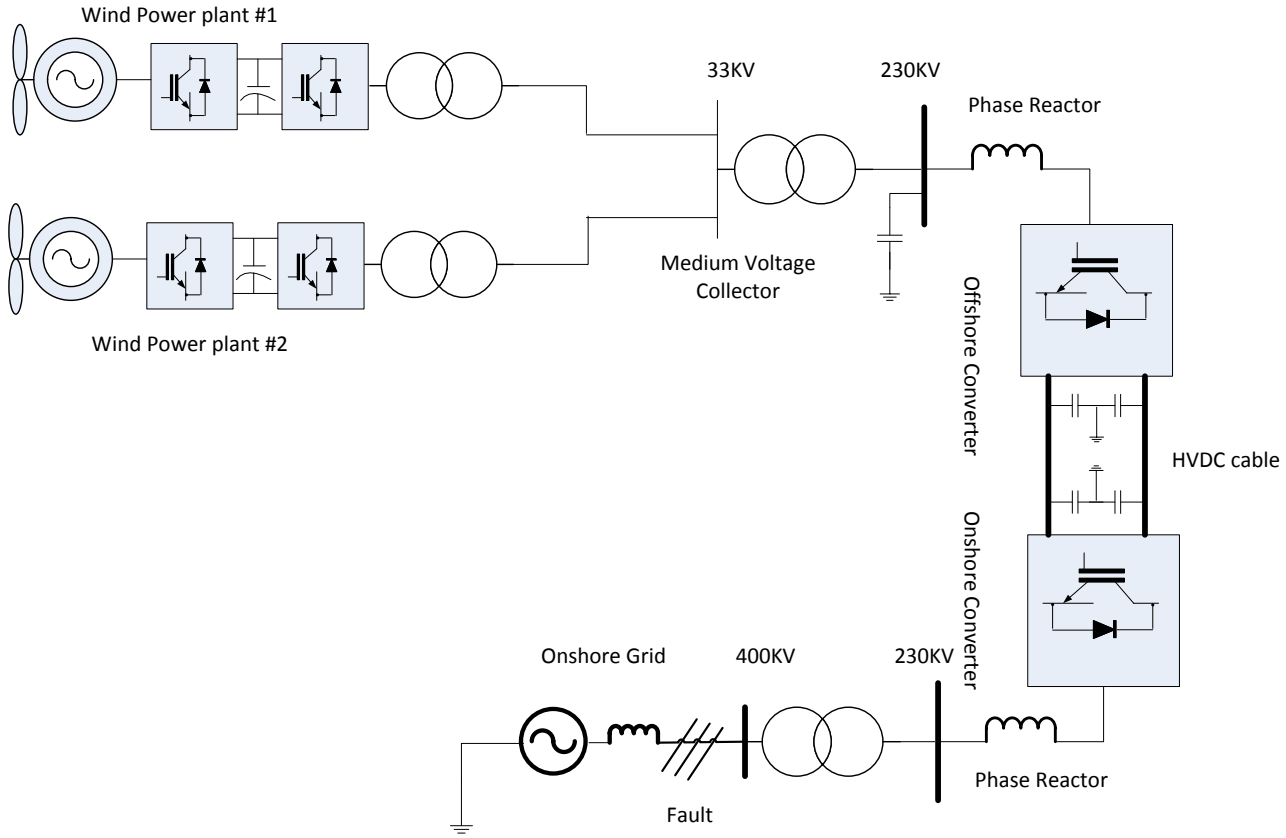

Figure 4.1: *Test system*

$$R_{grid} = Z_{grid} \cos\theta_g = 32 * \cos 84.3^\circ = 3.18\Omega \tag{4.2}$$

$$X_{grid} = Z_{grid} \sin\theta_g = 32 * \sin 84.3^\circ = 31.8\Omega \tag{4.3}$$

$$L_{grid} = \frac{X_{grid}}{\omega} = \frac{31.8}{2 * 50 * \pi} = 0.101H \tag{4.4}$$

where,

Z_{grid} is the grid impedance, V_{grid} is the rated grid voltage, P_n is the rated active power from OWFs, S_k is the short circuit ratio, R_{grid} is the grid resistance, θ_g is the grid angle, X_{grid} is the grid reactance, L_{grid} is the grid inductance.

4.1.2 Converter Transformer

Converter transformers are used to transform the voltage of ac system to a level suitable for converter. It can also provide some reactance between the converter and ac system to limit and control the ac current [29]. The offshore converter transformer has a nominal voltage ratio of 33/230 kV with 33kV connected to the offshore electrical collector. The onshore converter transformer has a nominal voltage ratio of 230/400 kV with 400 kV connected to onshore grid. The leakage reactance is assumed to be 14%. The transformer tap changer and saturation are not simulated in this thesis.

4.1.3 Voltage Source Converter

Different types of VSCs are available in the market, e.g. two-level converter, three-level converter and modular multi-level converter (MMC).

Two-level converter is the simplest type of three-phase VSC. It consists of six valves and each valve consists of IGBTs and anti-parallel diodes. Until 2012, most of the VSC-HVDC system built was based on the two-level converter [9]. It uses PWM technology to produce the control signal for turning on and turning off of IGBTs. The voltage at the ac output of each phase is switched between two discrete voltage levels: $+\frac{1}{2}U_d$ and $-\frac{1}{2}U_d$. As a result of PWM, the IGBTs is turned on and turned off many times in each cycle, which will result in high switch losses.

Not like two-level converter, which can only synthesize two discrete voltage level at the ac terminals of each phase: $+\frac{1}{2}U_d$ and $-\frac{1}{2}U_d$, three-level converter can synthesize three discrete voltage level: $+\frac{1}{2}U_d$, 0, and $-\frac{1}{2}U_d$. As a result, harmonic performance is improved in three-level converter. However, three-level converter becomes more complex, which will increase the cost. Besides, the design of three-level converter becomes difficult when the dc voltage is higher than 150kv [9].

MMC contains around 300 submodules connected in series in each valve. Therefore the harmonic performance is excellent and usually no filters are needed [9]. Another advantage of MMC is that PWM is not necessary, with the result that power losses are much lower than two-level converters. However, the control of MMC becomes much more complex than two-level converter. Besides, the submodules capacitors are large and bulky [30].

The comparison of different types converters are summarized in the following table 4.1.

Although three-level converter has less harmonics, and MMC even has much less harmonics and has low losses, the interest of this thesis is not harmonics study. This thesis will use two-level converter because of its simplicity and easy to implement. The switching frequency of PWM in the two-level converter is 2000 Hz in this thesis. The onshore converter and offshore converter also contain dc capacitor and phase reactor. Their function and parameters are described in the following part.

	operating principle	advantage	disadvantage
two-level converter	use PWM to produce control signal for IGBTs;synthesize two discrete voltage level	simplest and less expensive	harmonics and high switching loss
three-level converter	synthesize three discrete voltage level	less harmonics	more complex and design is difficult for high dc voltage
MMC	around 300 submodules connected in series in each valve; PWM is not necessary	harmonic performance is excellent;power losses are much lower	control is much more complex and submodules capacitors are large

Table 4.1: *Comparison of different types of converters*

The dc capacitor can keep power balance during transient conditions and maintain the dc voltage during the option of VSC. The dc capacitor is sized based on the dc voltage, power capacity of the converter, and time constant of the converter. The following equation is used to calculate the value of dc capacitor:

$$\tau = \frac{CV_d^2}{2P_{dc}} \tag{4.5}$$

where V_d is the dc-link voltage, which is 500 Kv in this thesis. P_{dc} is the nominal power of the converter, which is 500MW in this thesis. τ is the time constant used to charge the capacitor to the nominal dc voltage level when VSC is supplied with constant active power equals to P_{dc}. For the VSC-HVDC system in this project, a time constant of 5ms is used. Based on the equation and the parameters above, the capacitor size is calculated as 20 μF.

The phase reactor facilitates the control of the active power and reactive power flow by regulating the currents through them. They also act as a harmonics filter to filter out of the harmonics in the current and voltage waveform, and to limit the short circuit current [29]. A large phase reactor will lead to low current ripples, but it will slow down the dynamic of the converter. In this thesis, a phase reactor of 0.15 pu has been used and the corresponding inductance value is 0.051H.

4.1.4 DC Cable

Cross-linked Polyethylene (XLPE) cables are used in this VSC-HVDC transmission. XLPE has the advantage of strong mechanical strength, flexibility and low weight. The XLPE cable mainly consists of conductor, insulation, water barrier, armoring and outer sheath. The parameter for the cable and the numerical data

used in simulation is taken from [31]. During the simulation in PSCAD, the cable uses frequency dependent (phase) model. This model incorporates the frequency dependence of all line parameters. It is the most advanced time domain model available. Another advantage of frequency dependent (phase) model is that it is the most numerically accurate and robust cable model available anywhere in the world!

4.1.5 Offshore Wind Farms

There are two OWFs with capacity of 200MW and 300MW separately. They are simulated using aggregated models. Each aggregate model consists of a PMSG and a back-to-back converter. The back-to-back converter is VSC and its operation frequency is 2500Hz. The rated output voltage for the two PMSG is 0.69kV. The detailed parameters of the two PMSG are shown in Appendix B.

4.2 Start-up Sequence

A start-up operation of the OWF can be achieved relatively easily with VSC-HVDC transmission. The operation sequence is in the following way [13] [28]:

- At the beginning, the VSC-HVDC and the OWF grid is in de-energized state. When the onshore circuit breaker is closed, VSC-HVDC terminal gets connected to the onshore grid, the anti-parallel diodes in the VSC conducts, a large inrush current flow in to charge the dc capacitor and the cable.
- Then onshore VSC is enabled, the dc-link voltage is regulated to its reference value.
- After the VSC-HVDC dc voltage is stabilized, the offshore VSC is de-blocked, Its control ramps up the ac voltage and the offshore grid voltage gradually builds up. During this period, the power flows from onshore VSC to offshore VSC since a small amount of active power is need to supply the power losses in the offshore equipment and network.
- After the offshore grid voltage is established, the wind turbine generator is synchronized to the imposed ac grid. The power starts to flow from the offshore VSC to onshore VSC and finally flows to the onshore grid.

4.3 PSCAD setting

PSCAD is a very powerful power system simulation software, which is developed by the HVDC Research Centre, Canada. It is a very flexible user interface to the famous EMTDC solution engine.

Before testing the system under steady state, the parameters in PSCAD should be set properly. Project setting in PSCAD is very important. It has a large effect on the simulation speed, accuracy of the simulation results, and numerical oscillation problems of the system. Therefore proper project setting in PSCAD is quite crucial.

Some of the project setting parameters largely affect the simulation results in this thesis. It may be a common problem, so these parameters will be listed here.

Solution time step does not only affect the simulation speed, but also has a large effect on the system active power losses. It is decided based on the following equation [32]:

$$t_{max} = \frac{1}{f_{largest} * 10} \tag{4.6}$$

where, $f_{largest}$ is the largest switching frequency of PWM used in the project. For example, in this thesis, the switching frequency of PWM in wind turbine is 2500 Hz and the switching frequency in HVDC is 2000 Hz, 2500 should be used to calculate the solution time step. t_{max} is the maximum solution time step. The solution time step used in the simulation should be equal or smaller than this value.

Another important parameter is the parameter of network solution accuracy and numerical chatter suppression. If it is not set properly, the system will have numerical oscillation problems. In the beginning, the simulation of this system always has some numerical oscillation. Different methods have been tried, like retuning the controller, changing the parameters of phase reactor, but numerical oscillation still exists. Finally, when the parameters of network solution accuracy and numerical chatter suppression are changed properly, the numerical oscillation problem disappears. Detailed project setting information in PSCAD can be found in [33].

4.4 Steady State Operation

This session presents the simulation results under steady state operation. The system has been tested under several wind conditions.

The wind condition for OWF1 is summarized as following:

- At beginning, the wind speed Vw is 10m/s, which is below the nominal wind speed which is selected as 12m/s.
- At t=10s, a ramp occurs which increases the wind speed Vw at a rate of 4m in 30s.
- At t=15s, a wind speed gust occurs which decreases the wind speed Vw amplitude 3m/s with 10s duration .
- Finally the wind speed reaches 14m/s which is higher than the nominal wind speed.

The wind condition for OWF2 is summarized as following:

- Wind speed Vw is kept at 10m/s, which is below the nominal wind speed which is selected as 12m/s.

There is a random fluctuation of wind speed in both OWF1 and OWF2. The detailed wind profile for OWF1 and OWF2 can be found in the Appendix C.

The simulation results are presented in three parts, the performance of OWF1, the performance of OWF2 and the performance of HVDC.

In the first part, it shows the wind profile of OWF1 in Figure 4.2 a), the power output in Figure 4.2 b), the pitch angle in Figure 4.2 c) and the dc voltage of the back-to-back converter in Figure 4.2 d). As is shown in Figure 4.2 a), the wind speed starts to increase from 10m/s at 10s, and at 15s a wind gust occurs, the wind speed decreases. After the gust, the wind speed increases again and finally reaches the steady state 14m/s. Figure 4.2 b) shows the output power of PMSG tracks the maximum power point. When there is a wind gust at 15s, the output power starts to decrease. After the gust, the output power increases again. When the wind speed reaches and exceeds the nominal speed, 12m/s, the output power keeps at 1 pu. It can be seen from Figure 4.2 c) that the pitch angle keeps at zero when wind speed is lower than 12m/s. When wind speed exceeds 12m/s, the pitch angle starts to increase to keep the output power at 1pu. Finally Figure 4.2 d) shows that the dc-link voltage between the back-to-back converter is regulated to its reference, which is set at 1.2 pu.

In the second part, it shows the performance of OWF2. The wind profile is shown in Figure 4.3 a). The power output is shown in Figure 4.3 b). The pitch angle is shown in Figure 4.3 c) and the dc voltage of the back-to-back converter is shown in Figure 4.3 d). From Figure 4.3 a), it can be seen the wind speed is kept at 10m/s, but there is a random fluctuation of wind speed. Figure 4.3 b) shows the output power of PMSG tracks the reference power point, which is around 0.6 pu. Because wind speed is below nominal speed, pitch angle is kept at zero degree, which is shown in Figure 4.3 c). Finally Figure 4.3 d) shows that the dc-link voltage between the back-to-back converter is regulated to its reference, which is set at 1.2 pu.

In the third part, the behavior of HVDC will be illustrated. Figure 4.4 a) shows the instantaneous offshore ac voltage. Figure 4.4 b) shows the offshore grid frequency. Figure 4.4 c) shows the active power flowing into the offshore converter. The dc voltage of onshore converter is shown in Figure 4.4 d). The active power flowing into the onshore grid is shown in Figure 4.4 e). Figure 4.4 f) shows the reactive power flowing onshore. Figure 4.4 a) and b) shows that the offshore converter can generate a three-phase sinusoidal voltage with constant amplitude and frequency, which can behave like an infinite bus bar and all the power produced by OWFs will be absorbed by it. This proves the effectiveness of offshore converter controller. In Figure 4.4 c), the active power flowing into the offshore converter is the sum of the

power from the two OWFs. Figure 4.4 d) shows the dc voltage at the terminal of onshore converter can be regulated to its reference, which is set 1pu. In Figure 4.4 e), it shows the output active power from OWFs can be transmitted to the onshore grid. But there is some power losses. Figure 4.4 f) shows that in steady state the reactive power is controlled to its reference value 0 pu.

4.5 Summary

A test system comprising of OWFs and VSC-HVDC has been developed in this chapter. The parameters for main components of the test system have been determined. This chapter also listed some very important parameters for PSCAD setting. The system was tested under different wind conditions to show it worked well. In next chapter, several fault ride through methods will be discussed.

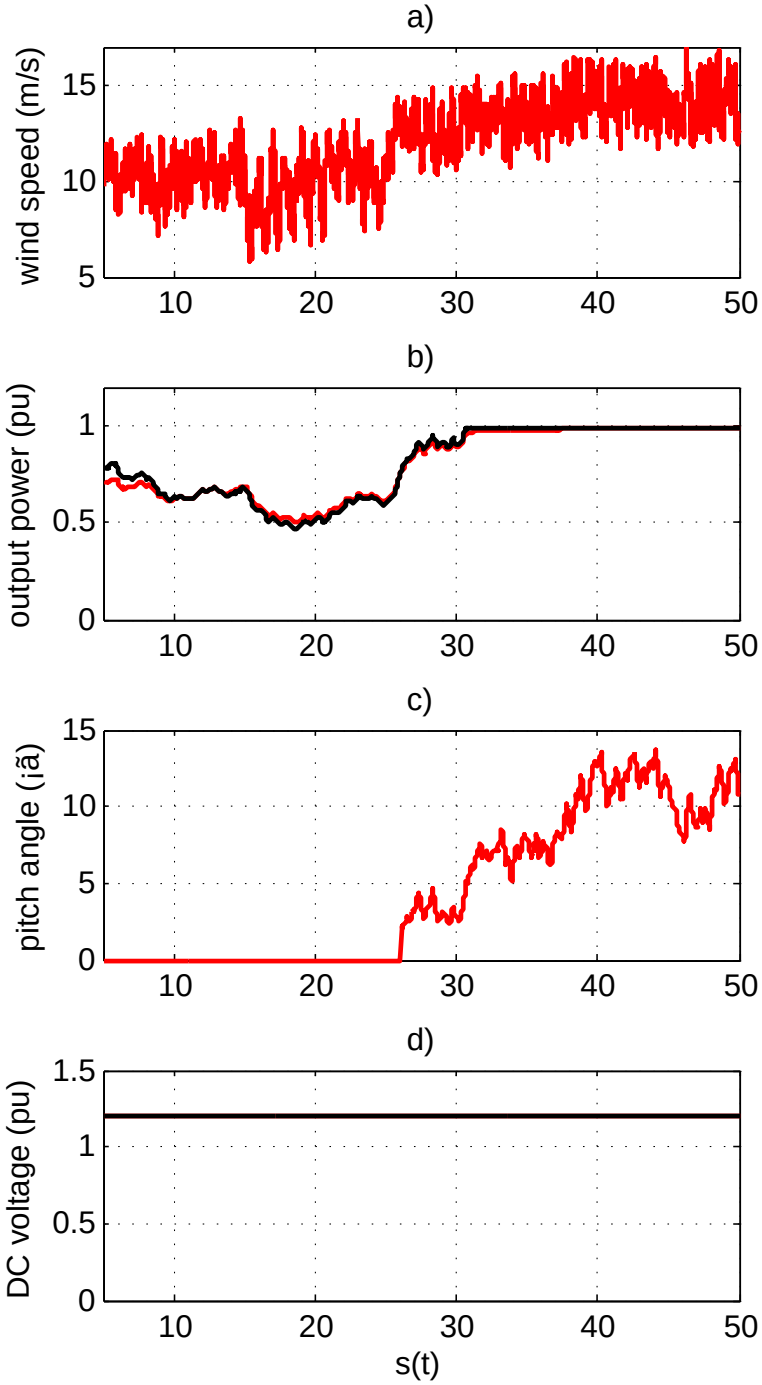

Figure 4.2: *Behavior of wind farm 1*

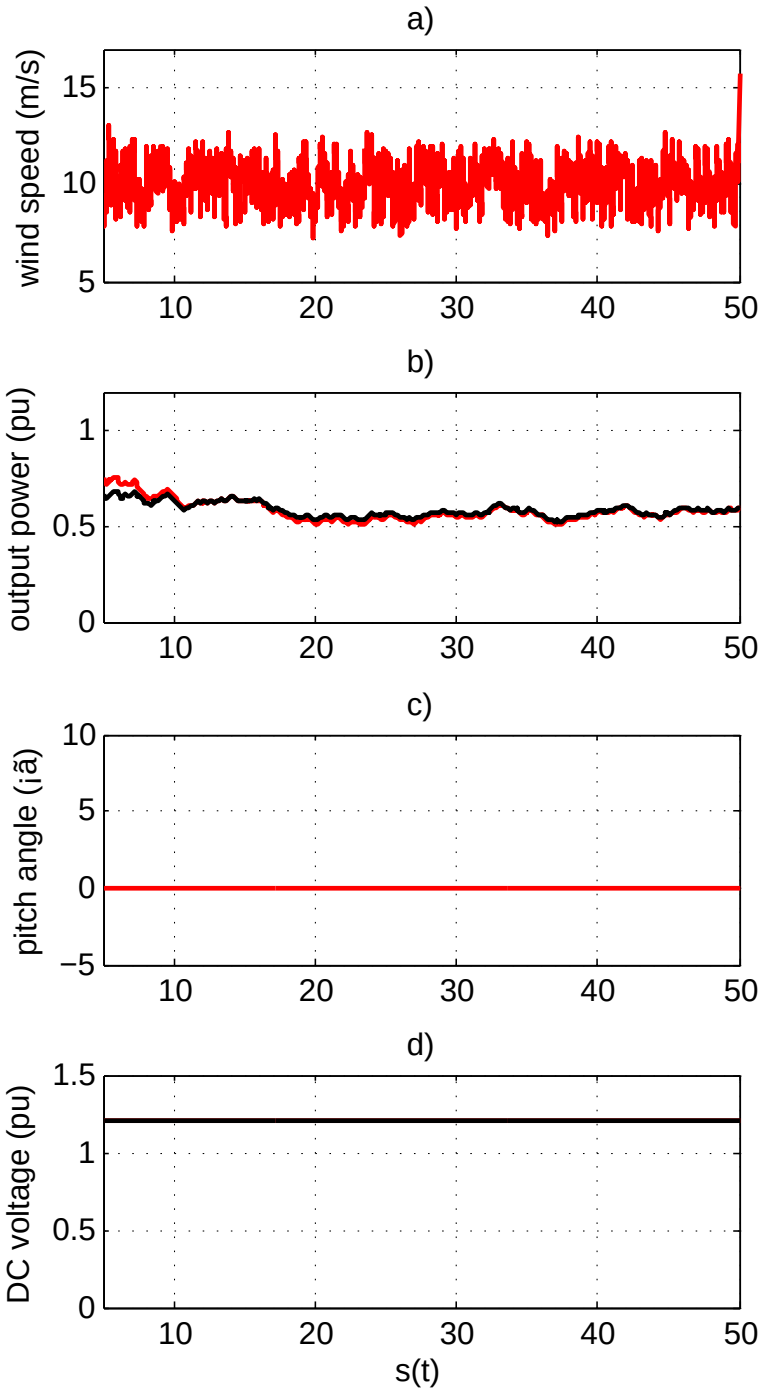

Figure 4.3: *Behavior of wind farm 2*

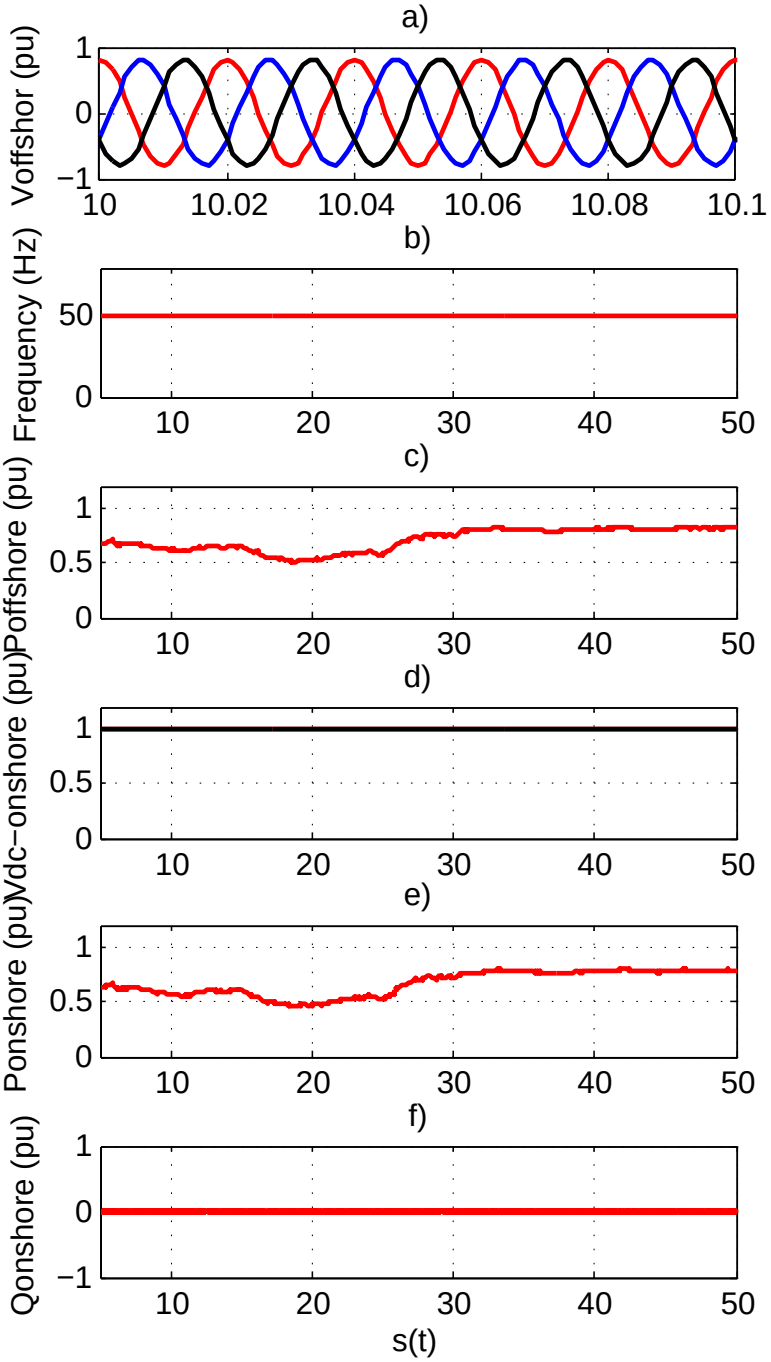

Figure 4.4: *Behavior of HVDC*

Chapter 5

Fault Ride through Methods and Simulation Results

This chapter mainly refers to different fault ride through (FRT) strategies as shown in following:

- Chopper resistor for FRT.
- Wind turbine power setpoint adjustment for FRT.
- Wind turbine active current control for FRT.
- Offshore voltage reduction for FRT.
- Enhanced FRT method.

It is organized as: first, a brief review of the German grid code requirement on FRT and reactive power compensation is presented. Then, the control ability of onshore converter to reactive power compensation during grid fault is tested. Next, the FRT methods listed above are described, including their theories, implementation, and effectiveness. Finally, the advantages and disadvantages of different FRT methods are compared and summarized.

5.1 Grid Code Requirement for Fault Ride Through

When wind farms (WFs) are connected to grid, many countries have regulations on the behavior of the WFs, e.g. FRT capabilities, reactive power control and voltage regulation. Some countries have developed grid codes to regulate the behavior of WFs, e.g. Danish grid code, German grid code, and Spanish grid code. German

grid code is well known and explained in different studies. The converter controller design in this thesis is based on German grid code, but the design principle of converter controller is the same for other grid codes. Refer to [34] for the grid codes from other countries.

Figure 5.1 shows the FRT requirement from Germany grid code [34] [28], summarized as following:

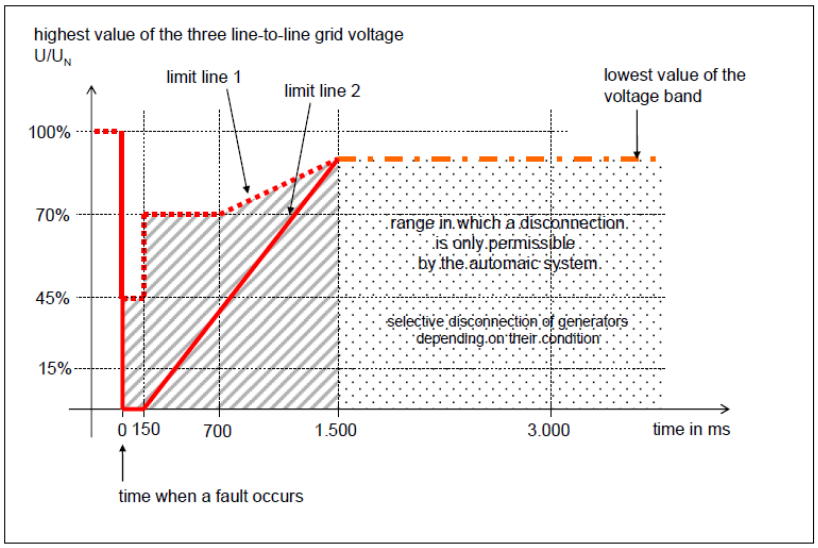

Figure 5.1: *Limit curve for FRT requirements of the German grid code [35]*

- Three-phase short circuits or fault-related symmetrical voltage dips must not lead to disconnection of the WFs when voltage is above limit line 1.
- Voltage drops within the area between limit line 1 and limit line 2 should not lead to disconnection of WFs, but in case of wind turbine instability or generator protection response, short-time disconnection is allowed.
- When voltage is below limit line 2, disconnection of the wind turbines is allowed. For all generating plants that donot disconnect from the grid during fault, the active power output must be continued immediately after fault clearance and increased to the original value with a gradient of at least 20% of the rated power per second.

Some grid codes also prescribe that WFs should support the grid by generating reactive power during a network fault, to support and restore the grid voltage. German grid code requires that the generating plants must support the grid voltage with additional reactive current during a voltage dip, as shown in Figure 5.2. The voltage control must take place within 20 ms after fault recognition by providing additional reactive current on the low-voltage side of the wind turbine transformer, amounting to at least 2% of the rated current for each percent of the voltage dip. A reactive power output of at least 100% of the rated current must be possible if necessary [34] [28]. In the case of OWFs the dead band is reduced to +5%.

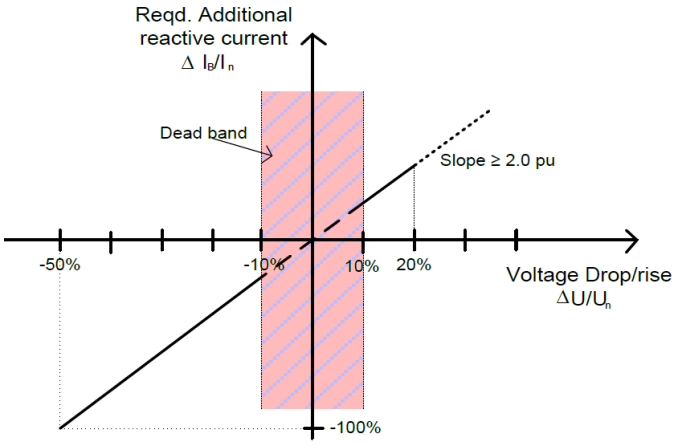

Figure 5.2: *Reactive output current during voltage disturbances according to German grid code [35]*

5.2 Reactive Power Compensation Performance of Onshore Converter

Just as mentioned in last section, some grid codes require that WFs should support the grid by generating reactive current during a network fault, to support and restore the grid voltage. Because reactive power compensation helps FRT, this section will evaluate the reactive power control ability of onshore converter during grid fault.

In this thesis, the onshore converter reactive power control is based on German grid code requirement of reactive current, shown in Figure 5.2. The control structure of onshore converter is shown in Figure 2.10.

In order to evaluate onshore converter control ability to reactive power during a network fault, a simulation study has been carried out on the test system shown in Figure 4.1 during a three-phase fault in the onshore grid. This fault occurs at 10.5s and last for 200ms, and a small ground fault resistance is used. Figure 5.3 shows onshore ac voltage, onshore d-axis current, and onshore q-axis current.

As can be seen from Figure 5.3, when a three phase fault occurs onshore, the onshore ac voltage decreases to nearly zero as is expected. In order to support and restore the grid voltage, reactive current changes from 0 to -1 pu which meet the German grid code reactive power requirement shown in Figure 5.2. As a result, active current reduces from 0.87 pu to 0. The performance shows that onshore converter controller is effective to control reactive current when onshore grid fault occurs.

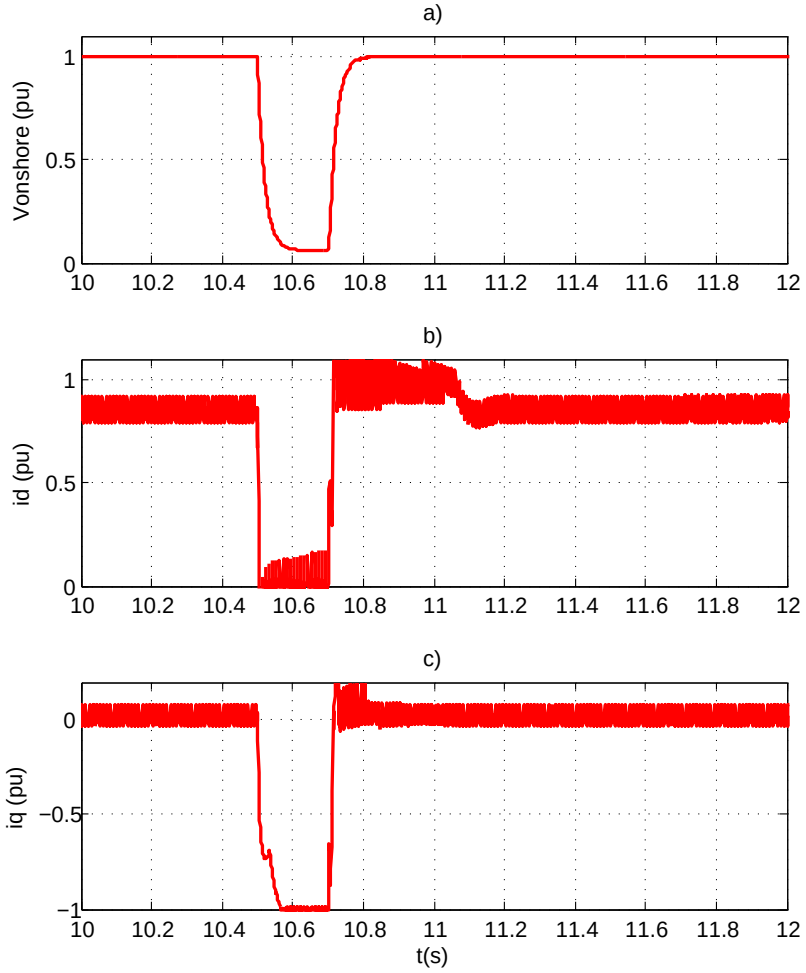

Figure 5.3: *Active current and reactive current changes of onshore converter during three phase fault*

5.3 Chopper Resistor for Fault Ride Through

A dc chopper consists of a dc resistor directly controlled through a power electronics switch, e.g. GTO, IGBT. It is installed in the VSC-HVDC onshore converter station as is depicted in Figure 5.4. The main function of dc chopper is to limit the dc voltage by dissipating the excess power as heat when a fault occurs at the ac grid. When the dc voltage exceeds its threshold value, in this thesis 1.1 pu is chosen, the power electronics, e.g. GTO, IGBT, is switched on. The power is dissipated by the resistor, and thus limit dc voltage rise within safety level. When the dc voltage is below its threshold value, the power electronics, e.g. GTO, IGBT, is switched off. This method is very straightforward and the behavior of the WFs is not affected by the fault, but a WF rated chopper resistor is likely very costly and it does not take the advantage of capability of the VSC-HVDC converter.

With the aid of Figure 5.4 , dc-link dynamics can be determined by the expression

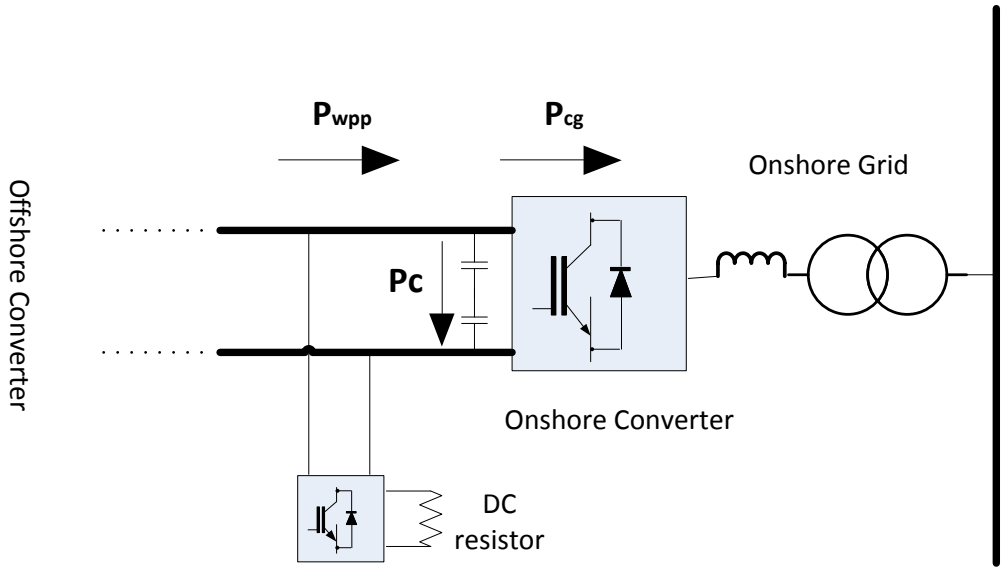

Figure 5.4: *Scheme of onshore DC chopper resistor*

as [36]:

$$P_C = P_{wpp} - P_{cg} \tag{5.1}$$

where,

P_C is the power that goes through the dc-link capacitor

P_{wpp} is the power flow from WFs

P_{cg} is the power flow to onshore grid.

The power flow through the capacitor is given by:

$$P_C = V_{dc} I_{dc} = V_{dc} C_{eq} \frac{d_{V_{dc}}}{d_t} = \frac{C_{eq}}{2} \frac{d_{V_{dc}^2}}{d_t} \tag{5.2}$$

where,

V_{dc} is the dc voltage of the dc-link

I_{dc} is the dc current flowing into the capacitor

C_{eq} is the equivalent capacitance of HVDC cable and dc capacitor.

Rearranging and integrating both sides of the equation (5.2) as follows:

$$V_{dc} = \sqrt{\frac{2}{C_{eq}} \int (P_C) dt} \tag{5.3}$$

Substituting P_C by using equation (5.1), the dc-link voltage can be expressed as:

$$V_{dc} = \sqrt{\frac{2}{C_{eq}} \int (P_{wpp} - P_{cg}) dt} \tag{5.4}$$

If a three phase fault occurs at the onshore grid, the power transferred from the onshore converter to onshore grid P_{cg} will be zero as the onshore grid voltage drops to zero. Based on equation (5.4), the power flow from WFs P_{wpp} must be reduced or dissipated by chopper resistor, so that the dc voltage will not increase. Based on the power flow from WFs P_{wpp} and the dc-link voltage V_{dc}, the equivalent size of such resistor can be estimated.

Suppose, the rated power flow from WFs is P_{rated}, and the over voltage in the dc-link has to be restricted within 10% of the rated dc voltage, then the size of resistor is given by:

$$R_{chop} = \frac{(1.1 V_{dc_{rated}})^2}{P_{rated}} = \frac{(1.1 * 500)^2}{500} = 605\Omega \tag{5.5}$$

In order to evaluate the effectiveness of chopper controlled resistor method, a simulation study has been carried out on the test system during fault condition shown in Figure 4.1. There are different fault types, e.g. single phase to ground fault, double phase fault, and three-phase to ground fault. Three-phase to ground fault belongs to the category of symmetrical fault and it represents the most severe case, so the chopper resistor is tested under three-phase to ground fault situation. The FRT methods presented later will also be tested under this situation. The fault occurs at 10.5s and last for 200ms, and a small ground fault resistance is used. Figure 5.5 shows the comparison of onshore ac voltage, onshore active power, onshore dc-link voltage, onshore reactive power, resistor dissipated power without and with chopper resistor. The comparison of offshore dc-link voltage, offshore ac voltage, dc voltage between wind turbine back-to-back converter, wind turbine output power without and with chopper resistor is shown in Figure 5.6.

From Figure 5.5 a), a*),b),and b*), it can be seen, after a three phase fault occurs at 10.5s, the onshore ac voltage decreases to nearly zero as is expected, which results in zero active power output. Without chopper resistor, the dc-link voltage increases to 2.35 pu as shown in Figure 5.5 c). If chopper resistor is applied, the dc-link voltage is kept below 1.22 pu as shown in Figure 5.5 c*). Figure 5.5 d) and d*) show when onshore fault occurs, OWFs will produce reactive power to support grid voltage restoration. During the moment of onshore voltage recovering to normal value, there will be large reactive power drawn from OWFs. From Figure 5.6 g), g*), h),h*),i),i*), it can be seen, the offshore ac voltage and the behavior of OWFs will not be affected by implementing chopper resistor. This is a huge advantage of chopper resistor for FRT.

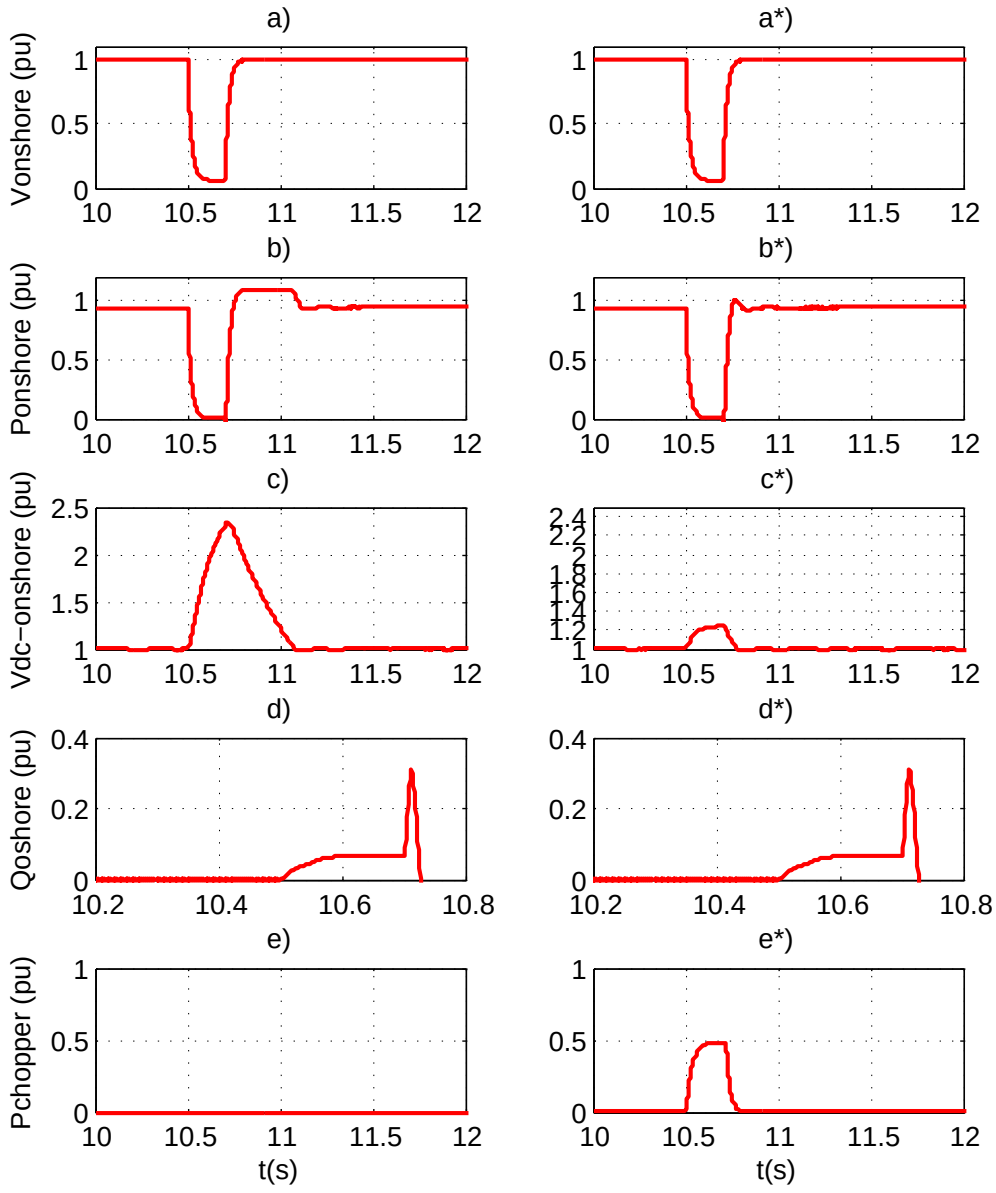

Figure 5.5: *Simulation results I during three phase fault without and with chopper resistor*

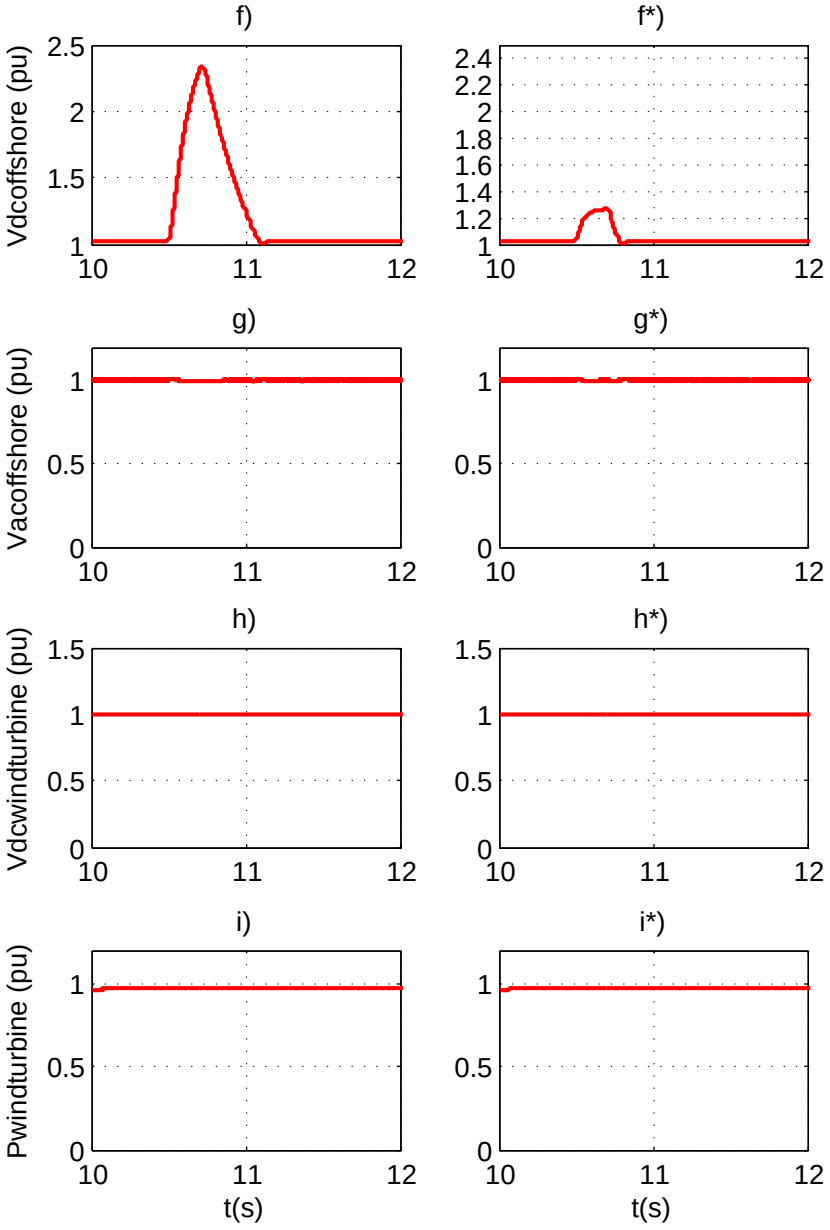

Figure 5.6: *Simulation results II during three phase fault without and with chopper resistor*

5.4 Wind Turbine Power Setpoint Adjustment for Fault Ride Through

The principle of this method is to reduce the power setpoint of each wind turbine when onshore fault occurs. The detail of this method is given below.

When an onshore grid fault occurs, the onshore ac voltage will decrease. When the onshore ac voltage decreases below a threshold value, in this thesis 0.9 pu is chosen, the power setpoint adjustment controller is activated. Because the onshore ac voltage decreases, the power transmitted from onshore converter to onshore grid is limited. This transmitted power limit is sent to the offshore converter via communication link. A power reduction factor for each wind turbine is calculated based on the power limit from onshore converter and the OWFs output power in offshore converter, as shown in the following:

$$K_p = \frac{P_{max}, OC}{P_o, WT} \tag{5.6}$$

where,

P_{max}, OC is maximum transmitted active power from onshore converter to grid in pu

P_o, WT is prefault total active power output of the OWF in pu.

The power reduction factor is sent to each individual wind turbine from offshore converter via communication link. This power reduction factor multiplies the prefault power reference to produce the new power setpoint for wind turbines. This new power setpoint is the power reference sent to GSC. In this thesis, the two aggregate models of OWFs represent two wind turbines to show the operation principle of this method. The control structure is shown in Figure 5.7.

A communication delay between onshore converter, offshore converter and wind turbines should be considered in this method.

The perceived communication delay between the onshore converter, offshore converter and wind turbines is of the order of 10ms-100ms [28]. In this thesis, a order of 30ms is selected.

In order to evaluate the effectiveness of power setpoint adjustment method, a simulation study has been carried out on the test system during a three-phase fault in the onshore grid shown in Figure 4.1. This fault occurs at 10.5s and last for 200ms, and a small ground fault resistance is used. Figure 5.8 shows the comparison of onshore ac voltage, onshore active power, onshore dc-link voltage, onshore reactive power without and with power setpoint adjustment method. The comparison of offshore dc-link voltage, offshore ac voltage, offshore active power, active power from OWF1 , and active power from OWF2 without and with power setpoint adjustment method is shown in Figure 5.9.

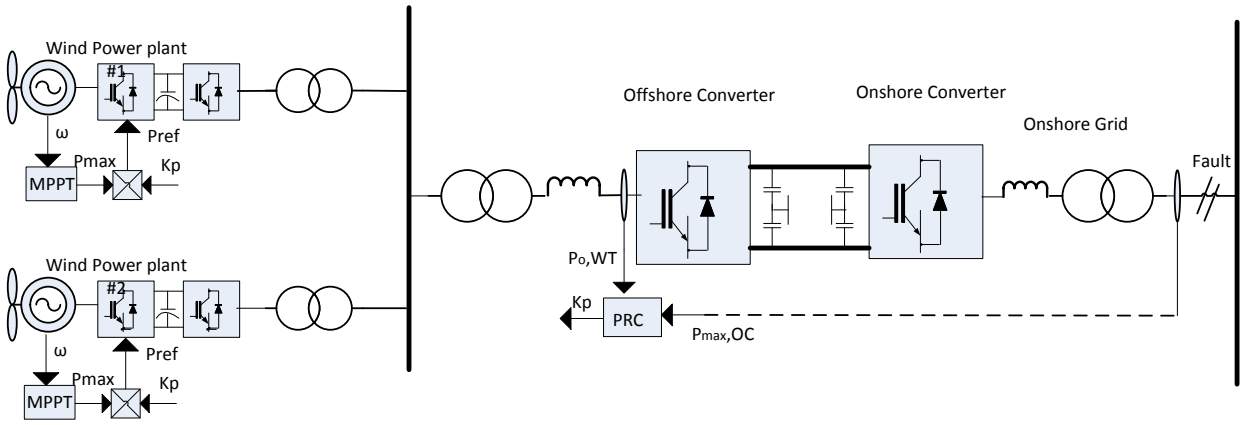

Figure 5.7: *Overall control structure of power setpoint adjustment method*

From Figure 5.8 a), a*),b),and b*), it can be seen, after a three phase fault occurs at 10.5s, the onshore ac voltage decreases to nearly zero as is expected, which results in zero active power output. Without power setpoint adjustment method, the dc-link voltage increases to 2.35 pu as shown in Figure 5.8 c). If power setpoint adjustment method is applied, the dc-link voltage reduces to 1.58 as shown in Figure 5.8 c*). Figure 5.8 d) and d*) shows when onshore fault occurs, OWFs will produce reactive power to support grid voltage restoration. During the moment of onshore voltage recovering to normal value, there will be large reactive power drawn from wind farms. Figure 5.9 f) and f*) shows, offshore ac voltage will not be affected by power setpoint adjustment method. From Figure 5.9 g), g*), h), h*), i), and i*), it can be seen, the offshore active power will drop from pre-fault value 475MW to 40MW, OWF1 active power drops from 290MW to 25MW, and OWF2 active power drops from 188MW to 17MW. These figures also show the active power from OWF1 and OWF2 donot drop immediately when the fault occurs at 10.5s, but with a delay.

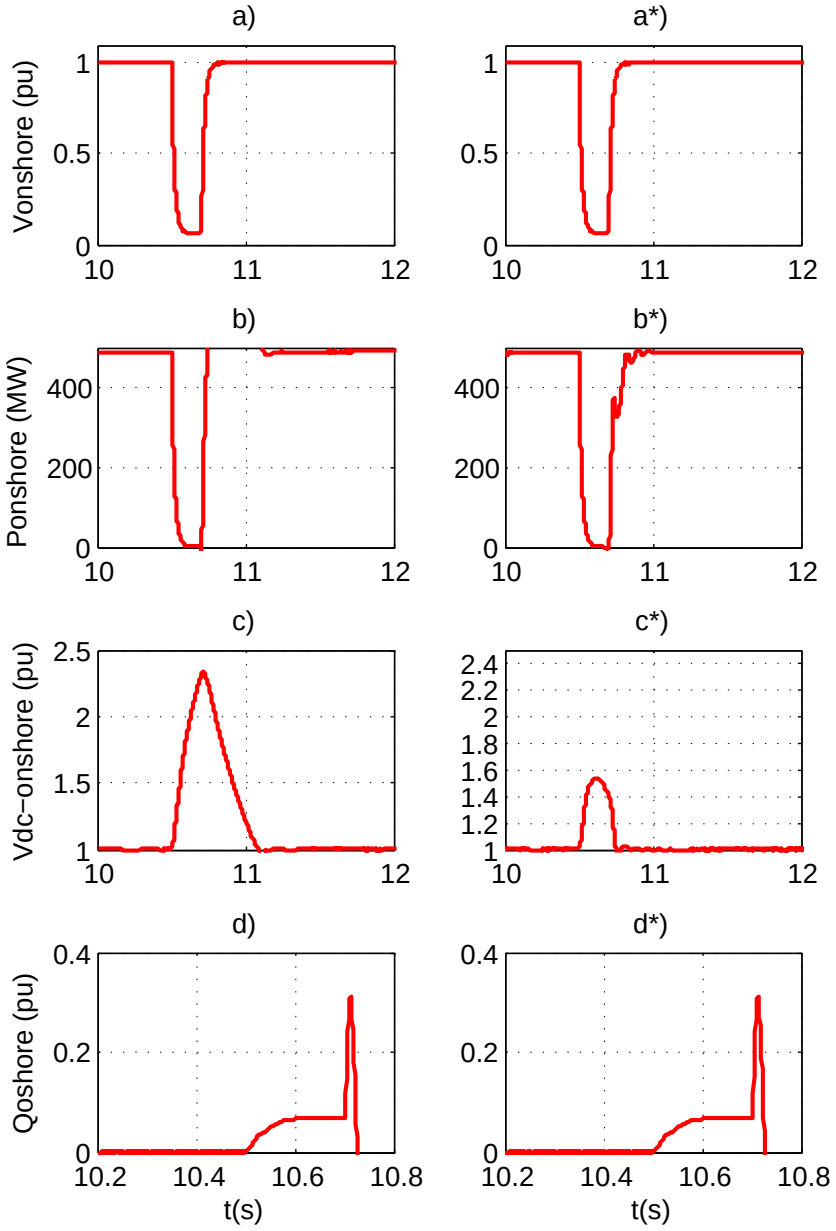

Figure 5.8: *Simulation results I during three phase fault without and with power setpoint adjustment method*

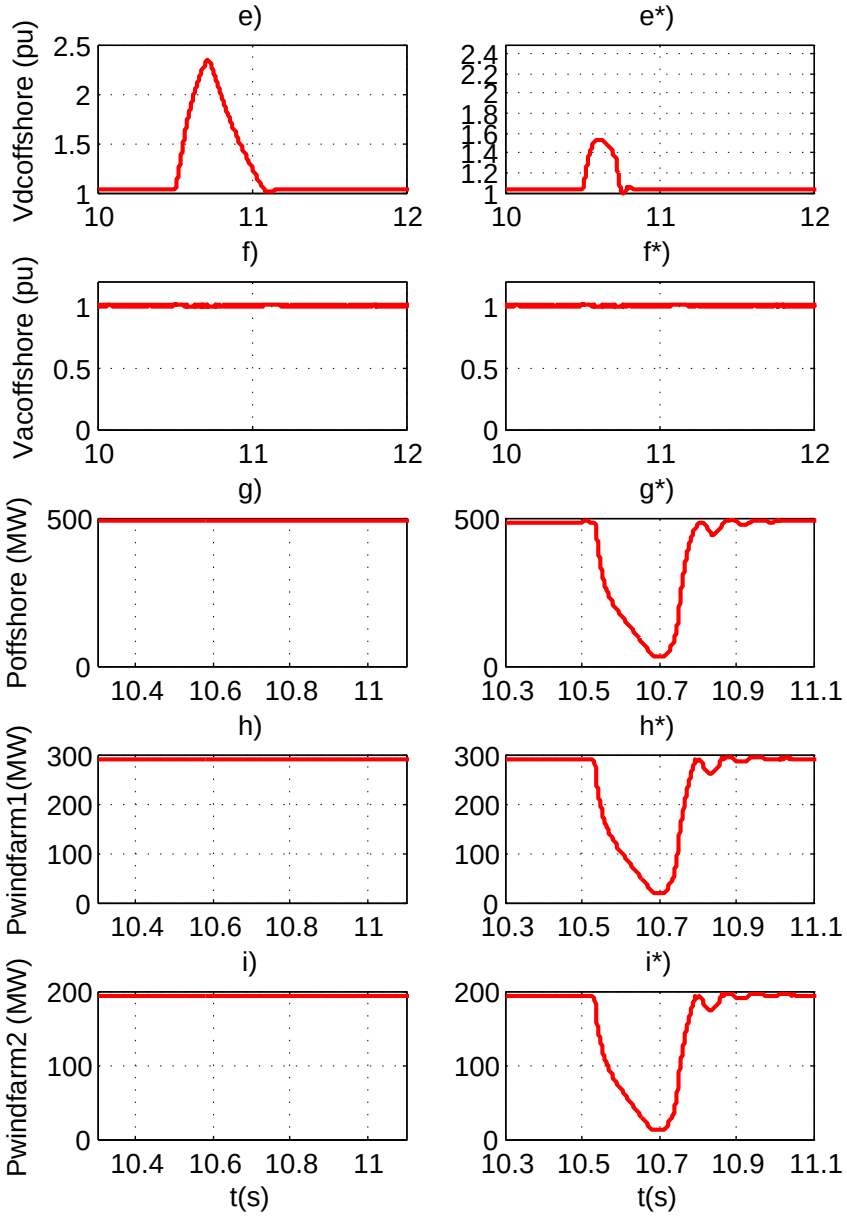

Figure 5.9: *Simulation results II during three phase fault without and with power setpoint adjustment method*

5.5 Wind Turbine Active Current Control for Fault Ride Through

Another FRT method is to block the wind turbine output power via wind turbines ACGSC control by reducing the active current components [37]. This can be implemented by adding a dc voltage droop to wind turbines ACGSC controller as shown in Figure 5.10. The HVDC de-loading droop introduces a multiplying factor into wind turbines grid side active current controller. When an onshore ac fault occurs, the HVDC-link voltage increases beyond its threshold value, in this thesis 1.1 pu is chosen. Then a reduction factor based on this increased dc voltage is sent to wind turbine ACGSC, and thus the wind turbines grid side active current is reduced to block the wind turbine output power. This method blocks the output power from the wind turbine which will increase the dc voltage between the back-to-back converter. And this will produce electrical stress on the wind turbine drive train. Because the reduction factor is sent from offshore converter to each wind turbine, a communication delay should be considered in this method.

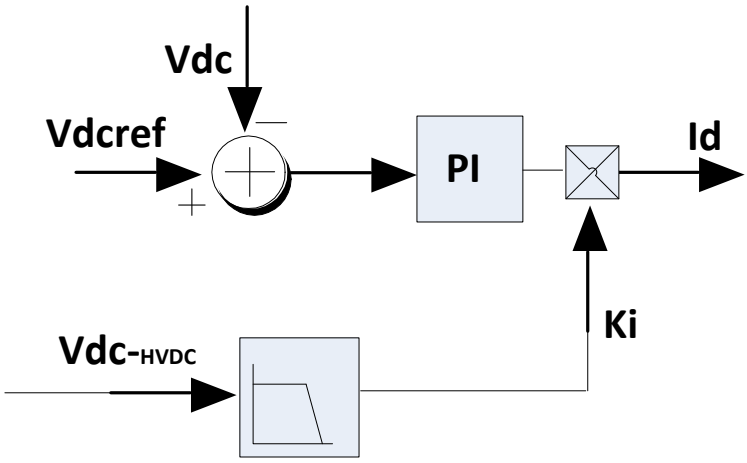

Figure 5.10: *De-loading wind turbine output power via wind turbine grid side controller*

The de-loading droop can be decided in this way: below dc voltage threshold, the droop gain K_i (see Figure 5.10) is one. K_i decreases linearly to zero as the dc voltage increases to a specific upper limit. HVDC over voltage control ability is related to the slope of the droop, shown in Figure 5.11. In other words, the HVDC over voltage control ability is related to the specific upper dc voltage limit, e.g. 1.2 pu, 1.3 pu, 1.4 pu, shown in Figure 5.11. When a larger upper dc voltage limit is chosen, e.g. 1.4 pu, the droop will have a smaller slope. As a result, the control ability of HVDC over voltage will be weak, but the electrical stress on wind turbine drive train will be small. When there is a smaller upper dc voltage limit, e.g. 1.2 pu, the droop will have a larger slope. As a result, the control ability of HVDC over voltage will be strong, but the electrical stress on wind turbine drive train will be large. Compromising the control ability of HVDC over voltage and the effect on wind turbine drive train, 1.3 is chosen as the upper limit in this thesis, as the red

line in Figure 5.11. The value of K_i will be decided by HVDC voltage following the red curve.

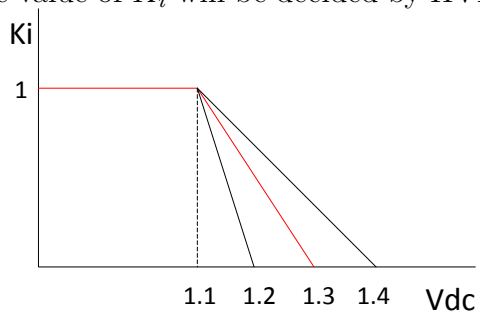

Figure 5.11: *HVDC de-loading droop*

In order to evaluate the effectiveness of active current control method, a simulation study has been carried out on the test system during a three-phase fault in the onshore grid shown in Figure 4.1. This fault occurs at 10.5s and last for 200ms, and a small ground fault resistance is used. Figure 5.12 shows the comparison of onshore ac voltage, onshore active power, onshore dc-link voltage, and onshore reactive power without and with offshore active current control method. The comparison of offshore dc-link voltage, offshore current, offshore active power, and wind turbine back-to-back converter dc voltage without and with active current control method is shown in Figure 5.13.

From Figure 5.12 a), a*),b),and b*), it can be seen, after a three phase fault occurs at 10.5s, the onshore ac voltage decreases to nearly zero as is expected, which results in zero active power output. Without active current control method, the dc-link voltage increases to 2.35 pu as shown in Figure 5.12 c). If active current control method is applied, the dc-link voltage reduces to 1.4 pu as shown in Figure 5.12 c*). Figure 5.12 d) and d*) shows when onshore fault occurs, OWFs will produce reactive power to support grid voltage restoration. During the moment of onshore voltage recovering to normal value, there will be large reactive power drawn from OWFs. From Figure 5.13 f) and f*), it can be seen the current from OWFs is reduced from around 500A to around 100A, when the active current control method is applied. As a result, the output active power from OWFs is reduce to 0.25 pu as shown in Figure 5.13 g*). Because the active power output from OWFs is blocked and the active power produced by generator does not decrease immediately, the dc voltage between back-to-back converter increase to 1.6 pu which is shown in Figure 5.13 h*).

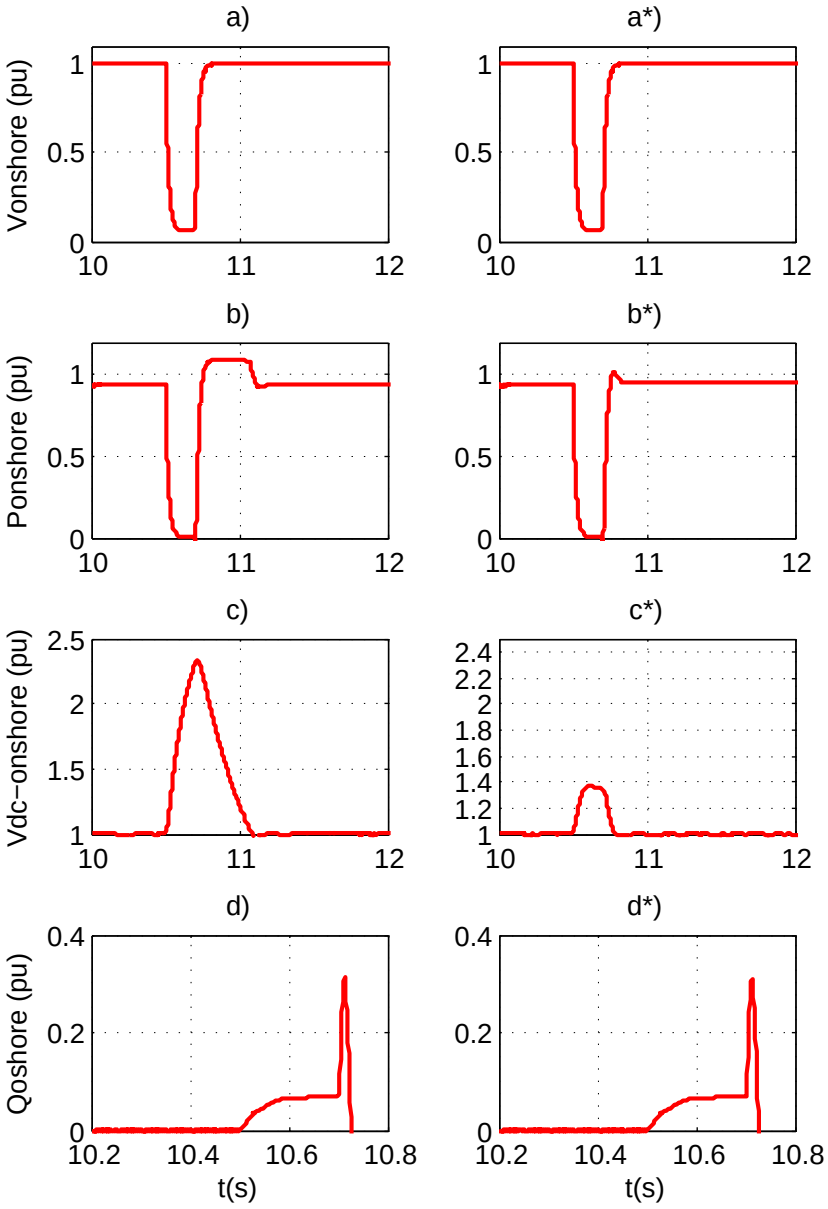

Figure 5.12: *Simulation results I during three phase fault without and with active current control method*

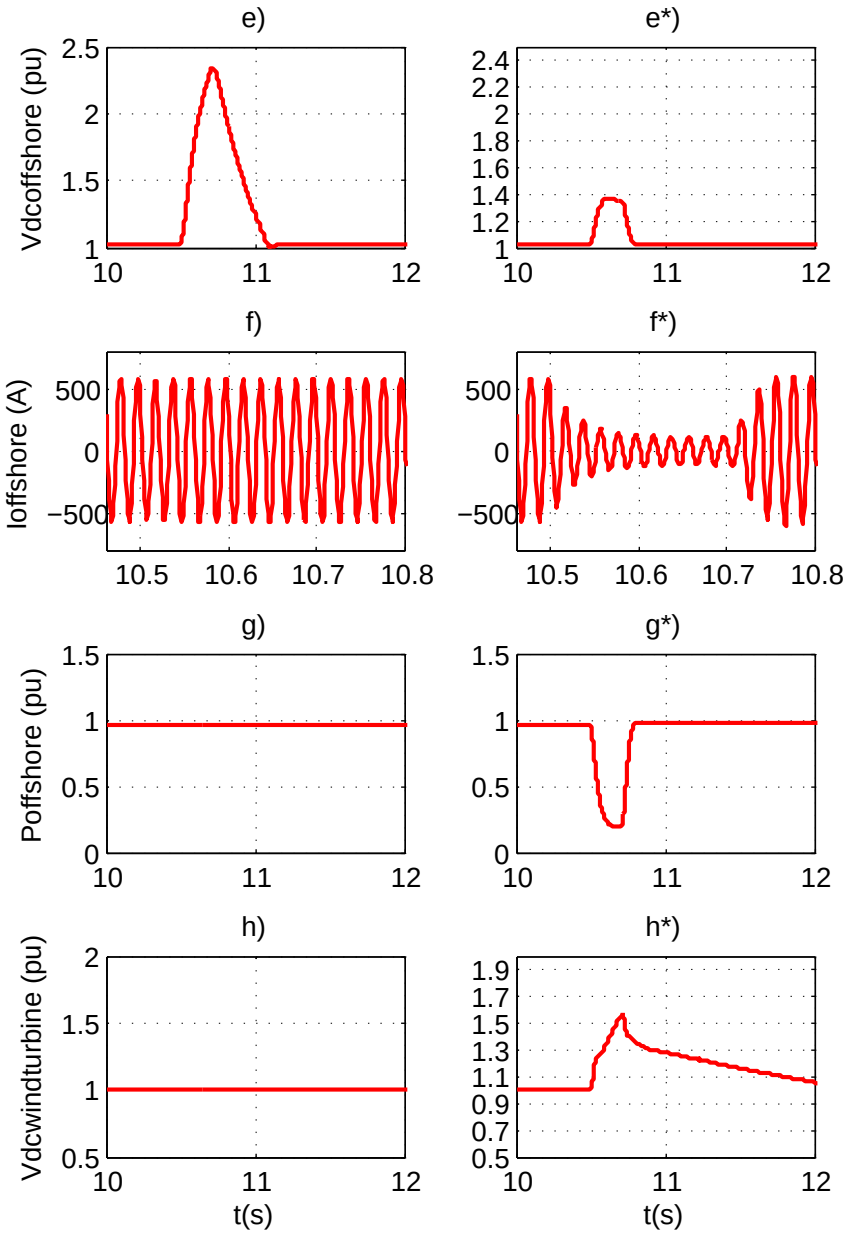

Figure 5.13: *Simulation results II during three phase fault without and with active current control method*

5.6 Offshore Voltage Reduction for Fault Ride Through

Another approach for FRT is to apply a fast voltage reduction in the OWF grid through offshore converter control. This enforces a very fast reduction of OWF power output and thus limits the dc voltage in a safety level. The fault detection can be implemented on the onshore ac grid side or on dc-link. The first measures ac voltage at onshore converter, and then calculate the required depth of the offshore voltage sag based on the onshore ac voltage, so it needs some communication time between onshore converter and offshore converter. The latter calculates the required depth of the offshore voltage sag by measuring dc voltage at offshore converter, so it needs no communication and has faster response [38]. This thesis adopts the latter method. The fault is detected on the dc-link voltage and the fault detection threshold value is 1.1 pu. It uses the increase of dc voltage to control the magnitude of the offshore converter output voltage. In order to realize this goal, a local control is included in the offshore converter station that proportionally decreases the ac voltage magnitude as a function of the dc voltage rise in the converter dc terminal [39].

Mathematically, the controller is described by:

$$V_{ac} = V_{ac_{ref}} - k_v(V_{dc_{ref}} - V_{dc}) \tag{5.7}$$

where V_{ac} is the calculated offshore ac voltage magnitude during fault, $V_{ac_{ref}}$ is the ac voltage magnitude reference during steady state, k_v is the droop gain that adapts the dc to the ac offshore voltage, $V_{dc_{ref}}$ is the steady state dc voltage reference and V_{dc} is the actual dc voltage magnitude. This calculated offshore ac voltage magnitude V_{ac} compares with the measured offshore ac voltage magnitude $V_{acmeasure}$ and the error is sent to PI controller to produce current reference. The implemented control block is shown in Figure 5.14 [40].

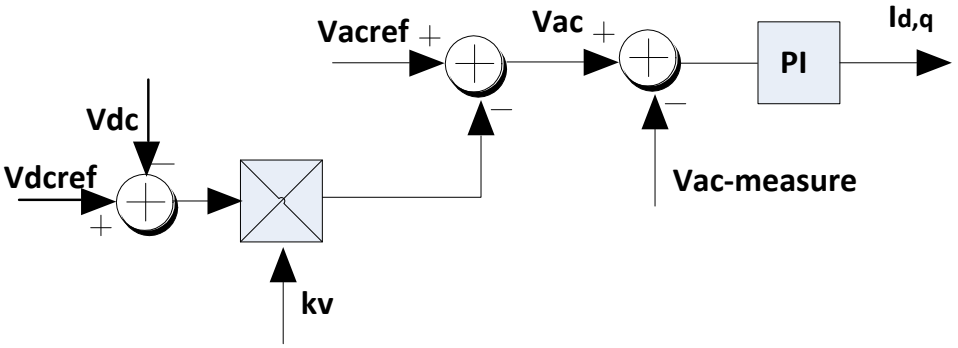

Figure 5.14: *Structure of offshore voltage reduction control*

This method requires no modification in the wind turbine control. Only the voltage support through reactive current during voltage sag is recommended to be deac-

tivated in wind turbine ACGSC [38]. Otherwise, it may lead to offshore voltage support that precludes the application of the envisioned control strategy.

In order to evaluate the effectiveness of offshore voltage reduction method, a simulation study has been carried out on the test system during a three-phase fault in the onshore grid shown in Figure 4.1. This fault occurs at 10.5s and last for 200ms, and a small ground fault resistance is used. Figure 5.15 shows the comparison of onshore ac voltage, onshore active power, onshore dc-link voltage, and onshore reactive power without and with offshore voltage reduction control. The comparison of offshore dc-link voltage, offshore ac voltage, offshore active power, and wind turbine back-to-back converter dc voltage without and with offshore voltage reduction control is shown in Figure 5.16.

Figure 5.15 a), a*),b),and b*) shows that, after a three phase fault occurs at 10.5s, the onshore ac voltage decreases to nearly zero as is expected, which results in zero active power output. Without offshore voltage reduction method, the dc-link voltage increases to 2.35 pu as shown in Figure 5.15 c). If offshore voltage reduction method is applied, the dc-link voltage reduces to 1.27 pu as shown in Figure 5.15 c*). Figure 5.15 d) and d*) shows when onshore fault occurs, OWFs will produce reactive power to support grid voltage restoration. During the moment of onshore voltage recovering to normal value, there will be large reactive power drawn from OWFs. Figure 5.16 f*) shows, the offshore ac voltage will reduce to 0.22 pu when offshore voltage reduction method is applied. As a result, the offshore active power decreases to 0.2 pu as shown in Figure 5.16 g*). The dc voltage between wind turbine back-to-back converter increase to 1.8 pu which is shown in Figure 5.16 h*).

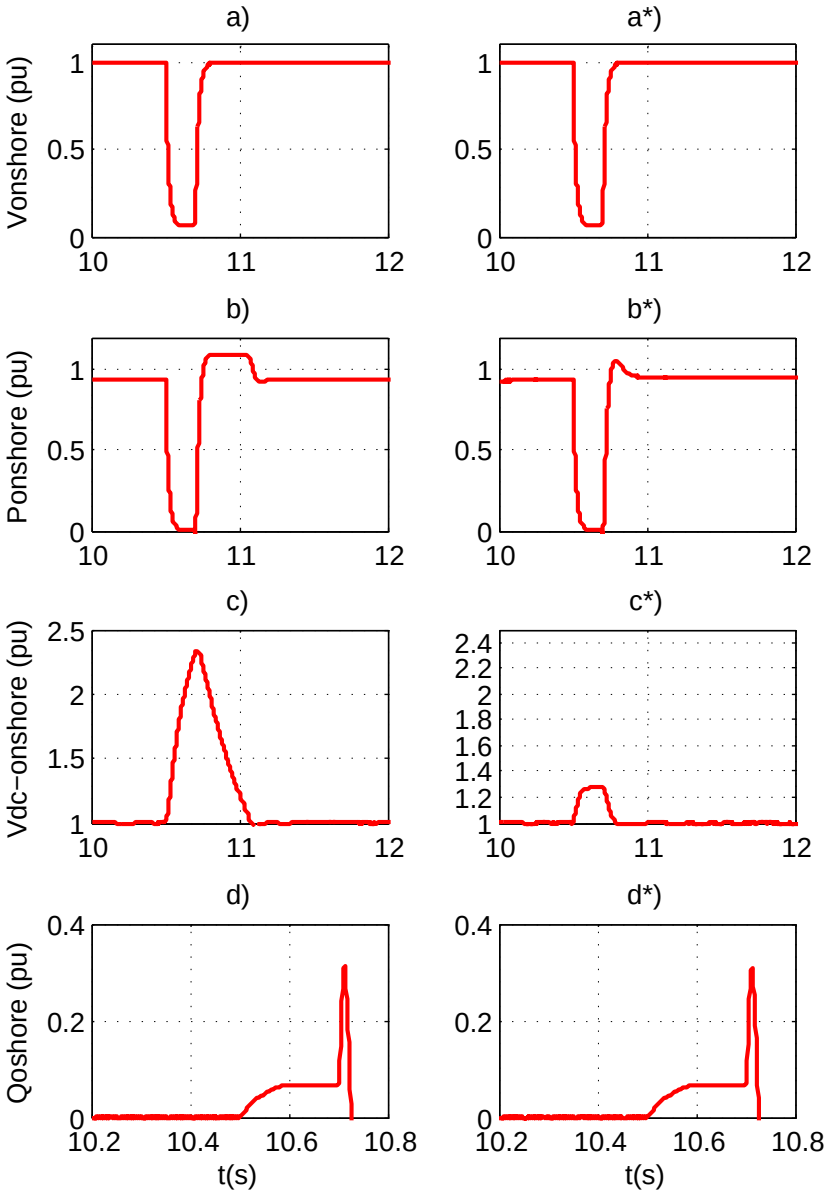

Figure 5.15: *Simulation results I during three phase fault without and with offshore voltage control method*

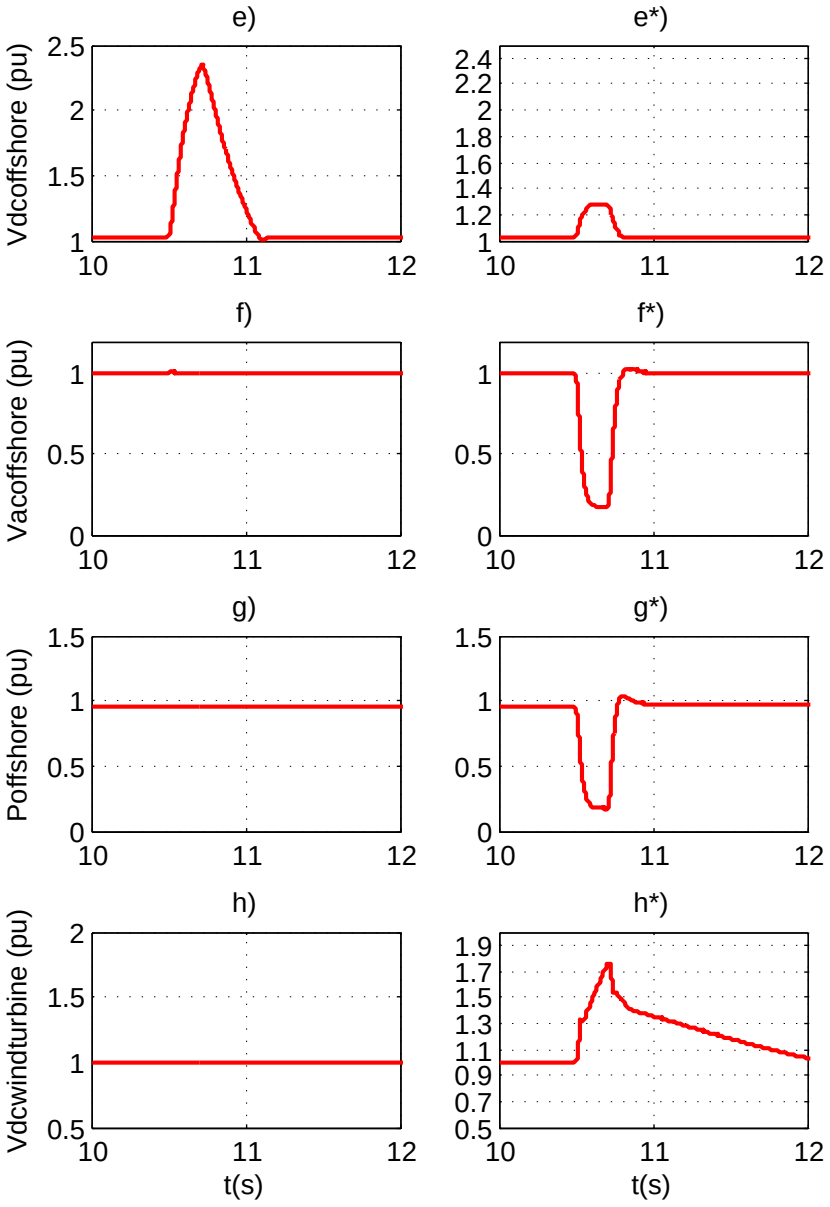

Figure 5.16: *Simulation results II during three phase fault without and with offshore voltage reduction control method*

5.7 Enhanced Fault Ride Through Method

As mentioned in previous section, chopper resistor can largely limit the HVDC-link voltage during onshore fault, but a large chopper resistor is very costly. The performance of power setpoint adjustment method highly depends on the communication speed and reliability of the communication link. Normally there is some communication delay between onshore converter, offshore converter, and individual wind turbine, so the effectiveness of this method is largely reduced. The performance of offshore active current control method is also affected by the communication delay between offshore converter and individual wind turbine. Offshore voltage reduction method can achieve fast power reduction, and thus limit the dc voltage increase value when onshore fault occurs. However, a fast power reduction offshore leads to a similar phenomenon like a OWF grid fault [38]. As a result, the power produced by the generator cannot be transmitted to offshore grid. It will result in the dc voltage increase between the back-to-back converters, which produces electrical stress on the wind turbine drive train.

The enhanced FRT method proposed here is based on power setpoint adjustment method and offshore voltage reduction method, but it eliminates the communication delay and electrical stress on the wind turbine drive train. The control ability of HVDC-link voltage during onshore fault is largely improved. It will be explained in the following section in detail.

The overall control structure is shown in Figure 5.17, When an onshore fault occurs, the dc voltage at the offshore converter will increase. When the dc-link voltage exceeds its threshold value, in this thesis 1.1 pu is chosen, it will activate the offshore converter controller to control offshore ac voltage magnitude, implemented by block VRC, based on equation (5.7). Almost at the same time, wind turbines detect the offshore ac voltage magnitude reduction. This will activate the wind turbine local controller. A power droop factor is generated and sent to GSC to deload active power. The power droop factor is decided by rated offshore ac voltage magnitude and reduced offshore ac voltage magnitude, implemented by block PRC, based on the following equation (5.8).

$$K_p = \frac{V_{reduce}}{V_{rated}} \tag{5.8}$$

where

K_p is the power droop factor,

V_{reduce} is the reduced offshore ac voltage magnitude,

V_{rated} is the rated offshore ac voltage magnitude.

This reduction factor can also be implemented on the active current controller of GSC, shown in Figure 5.18. By controlling the active current instead of controlling the power setpoint, the system has faster response.

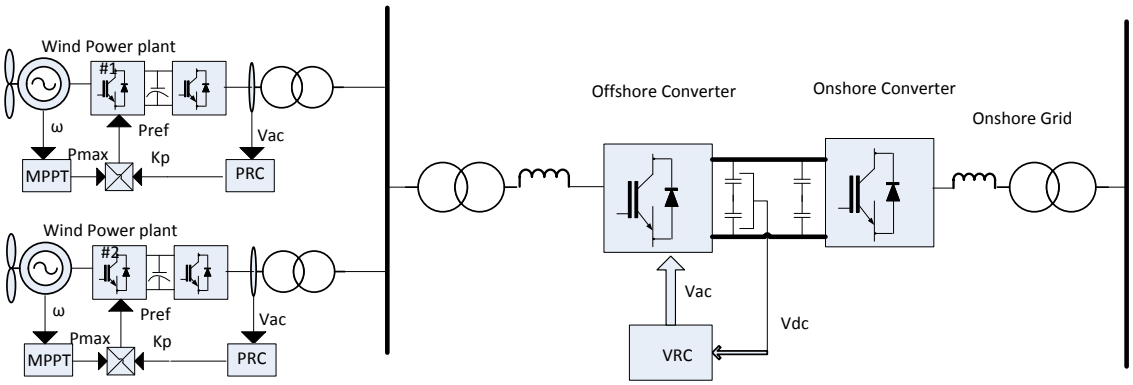

Figure 5.17: *Control structure of enhanced fault ride through method*

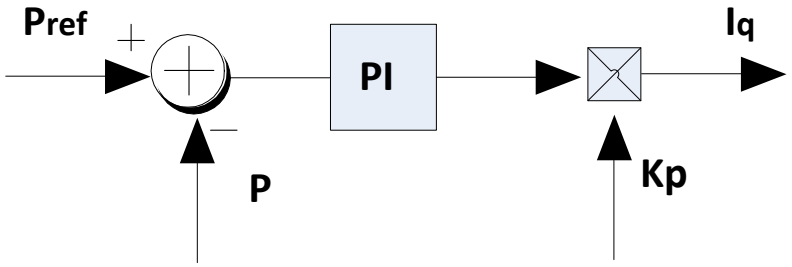

Figure 5.18: *Enhanced fault ride through method for current reduction*

There are three advantages of this enhanced FRT method:

First, in previous FRT methods [28] [38] [37], the power reduction factor for wind turbine is sent either from onshore converter by detecting the onshore ac voltage or from offshore converter by detecting the increase of HVDC-link voltage. These methods will have communication delay which limits the speed of power reduction. But in this new method, the power reduction factor is directly calculated from the wind turbine based on the offshore voltage reduction, so there is no communication delay.

Second, offshore voltage reduction behaves like a fault within the OWF grid, which

will lead electrical stress on the wind turbine drive train. This new method combines offshore voltage reduction method and wind turbine power reduction method. As a result, the dc voltage increasing in HVDC is limited, and at the same time, the wind turbine drive train does not suffer from large electrical stress.

Third, with this enhanced method, when an onshore fault occurs, the power sent to offshore converter is blocked by offshore voltage reduction. Almost at the same time, the output power from each wind turbine is also reduced by adjusting the wind turbine power setpoint or reducing the active current. The combined power reduction will largely improve the control ability of HVDC over voltage and limit the dc voltage within safety value.

In order to evaluate the effectiveness of enhanced FRT method, a simulation study has been carried out on the test system during a three-phase fault in the onshore grid shown in Figure 4.1. This fault occurs at 10.5s and last for 200ms, and a small ground fault resistance is used. Figure 5.19 shows the comparison of onshore ac voltage, onshore active power, onshore dc-link voltage, and onshore reactive power without and with enhanced FRT method. The comparison of offshore dc-link voltage, offshore ac voltage, offshore active power, wind turbine back-to-back converter dc voltage, and wind turbine active power output without and with enhanced FRT method is shown in Figure 5.20.

Figure 5.19 a), a*),b),and b*) shows that, after a three phase fault occurs at 10.5s, the onshore ac voltage decreases to nearly zero as is expected, which results in zero active power output. Without enhanced FRT method, the dc-link voltage increases to 2.35 pu as shown in Figure 5.19 c). If enhanced FRT method is applied, the dc-link voltage reduces to 1.2 pu as shown in Figure 6.19 c*). Figure 5.19 d) and d*) shows when onshore fault occurs, OWFs will produce reactive power to support grid voltage restoration. During the moment of onshore voltage recovering to normal value, there will be large reactive power drawn from OWFs. When enhanced FRT method is applied, offshore ac voltage is reduced to 0.2 pu as shown in Figure 5.20 f*). Accordingly offshore active power is reduced to 0.22 pu shown in Figure 5.20 g*). When wind turbine detects offshore voltage reduction, a power reduction factor will be applied to the generator side power control, the active output power from each wind turbine is reduced without almost no delay, as shown in Figure 5.20 i*). Compared to offshore voltage reduction method and active current control method, the dc voltage between wind turbine back-to-back converter increase to 1.23 pu, which is much lower than that with the other two methods.

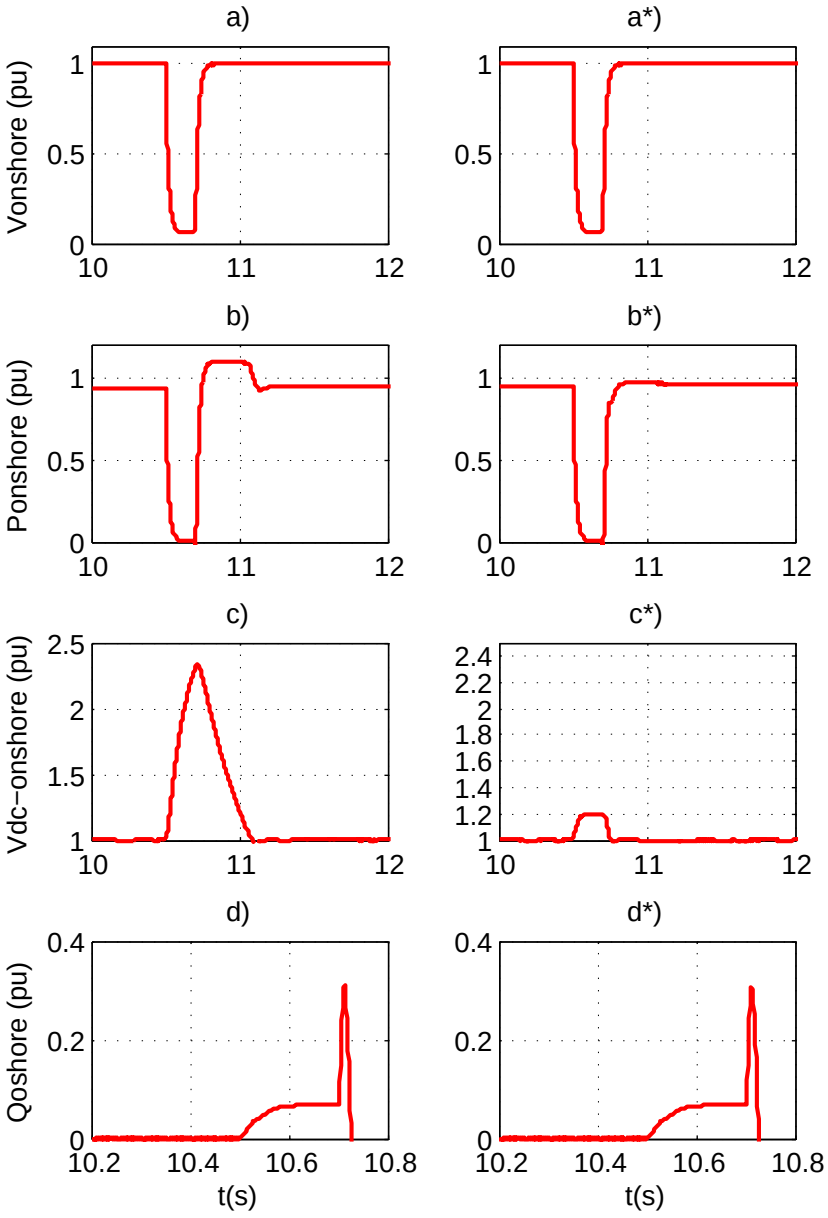

Figure 5.19: *Simulation results I during three phase fault without and with enhanced fault ride through method*

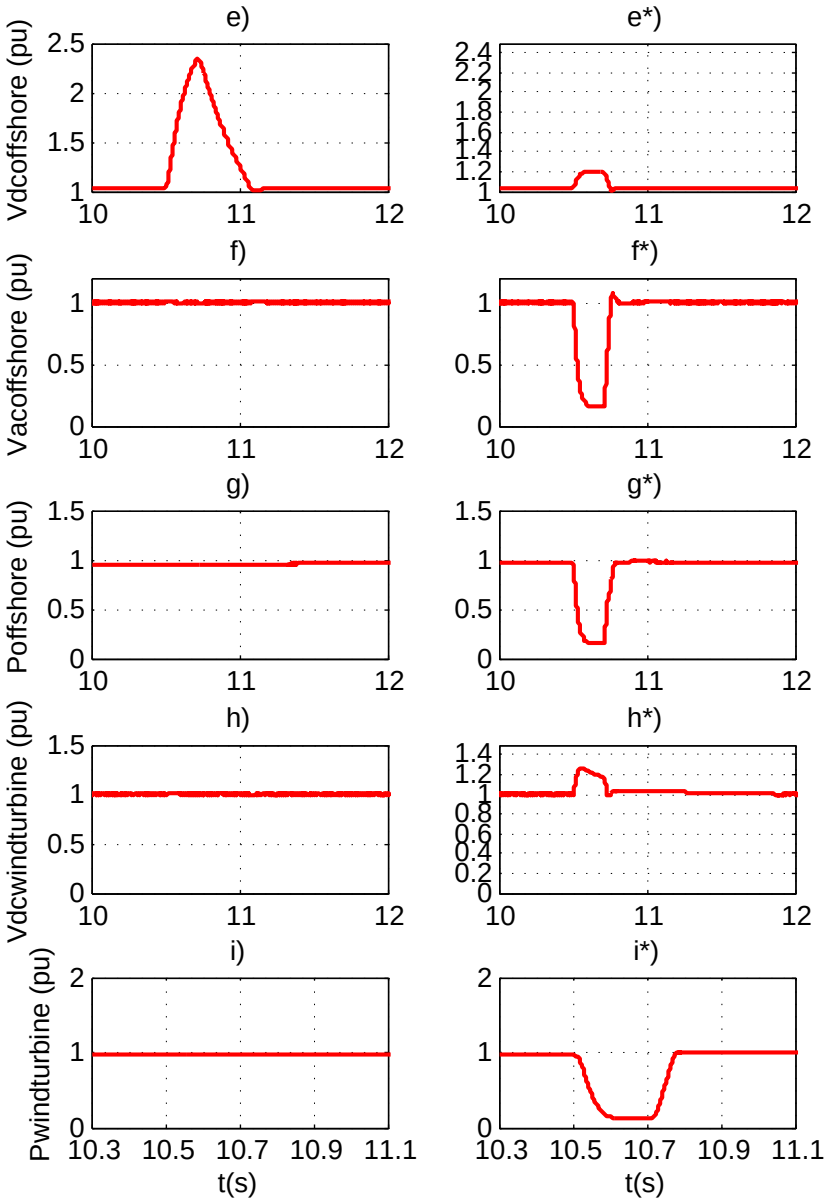

Figure 5.20: *Simulation results II during three phase fault without and with enhanced fault ride through method*

5.8 Summary

In section 5.3-5.7, five possible FRT methods for OWF connected to main grid via VSC-HVDC are described. In this section, five different FRT methods are compared.

FRT of OWFs connected to grid via VSC-HVDC can be achieved by using a chopper resistor. The extra energy in the dc-link can be dissipated by chopper resistor, so that dc voltage can be limited within a safety value. The main advantage of this approach is that OWFs stay completely unaffected by the fault, e.g. the output power from wind turbines remains constant during fault [38]. However, a large chopper resistor is very costly. FRT can also be achieved by de-loading the output power from each wind turbine with power setpoint adjustment method and active current control method. Both of these two methods are implemented by sending a de-loading signal to each wind turbine when fault occurs, but with the first method, the de-loading signal is sent to wind turbine GSC to control the power directly. With the latter method, the de-loading signal is sent to wind turbine ACGSC to control active current. These two methods do not affect the offshore grid voltage, but there is some communication delay, which will reduce the effectiveness of these two methods. Another approach for FRT is to reduce offshore grid voltage, so that less power is transmitted to HVDC-link. As a result, the dc-link voltage will be limited to safety level. This approach is realized via offshore converter control by measuring the dc-link voltage. So there is no communication delay, but wind turbines still produce power, if the power can not be transmitted to HVDC-link, extra power will accumulate in wind turbine drive train, which will result in electrical stress. The enhanced method for FRT combines de-loading each wind turbine and reducing offshore grid voltage. When onshore grid fault occurs, the offshore converter controller will reduce offshore grid voltage magnitude based on the increased dc-link voltage. Then power transmitted to HVDC-link will be reduced. Almost at the same time, each wind turbine detects the reduced offshore grid voltage. Based on this reduced offshore voltage and rated offshore voltage, a de-loading signal will be generated and sent to GSC. As a result, the output power from each wind turbine will be reduced. Compared with offshore voltage reduction method, there will be no extra power accumulating in wind turbine drive train. Another advantage of this method is no communication delay for sending de-loading signal to each wind turbine. There is also some limitations of this enhanced method, for example, if the offshore grid voltage reduction is not detected by wind turbine precisely, the performance of this method will be affected. The summary is shown in the following table 5.1.

	Fault ride through is achieve by	advantage	disadvantage
Chopper resistor	External resistor on HVDC link	It does not affect the behavior of wind turbines	A great amount of extra investment
Power setpoint adjustment	Sending signal to GSC and reducing each wind turbines' output power	It does not affect the offshore grid voltage	Communication delay and rely on the reliability of communication link
Active current control	Sending signal to wind turbine grid side converter and reducing each wind turbines' output power	It does not affect the offshore grid voltage and easy implementation	Communication delay and electrical stress on wind turbine drive train
Offshore voltage reduction	Decreasing offshore grid voltage and blocking the output power from wind turbines	No communication delay, very fast reduction of OWFs output power	Electrical stress on wind turbine drive train
Enhanced method	Decreasing offshore grid voltage and at the same time reducing the output power form each wind turbine	No communication delay, very fast reduction of OWFs output power, no electrical stress on wind turbine drive train, advanced control ability of HVDC over voltage.	If the offshore grid voltage reduction is not detected by wind turbine precisely, the performance of this method will be affected.

Table 5.1: *Comparison of different fault ride through methods*

Chapter 6

Conclusion and Future Work

6.1 Conclusion

VSC-HVDC appears to be a feasible and promising technology for connecting OWFs to onshore grid. However, when a fault occurs at onshore grid, power transmitted from onshore converter to onshore grid will be reduced depending on the severity of the fault, while the wind turbines still produce power. This unbalanced power will charge the dc capacitor and increase the dc voltage rapidly, which may expose the dc equipment to danger situation. The research work described in this thesis had the objective of designing FRT methods for OWFs connected to main grid via VSC-HVDC technology.

PMSG with full scale power converter is used in this thesis. The GSC is controlled to tract the maximum power, while ACGSC is controlled to regulate the dc voltage and reactive power. Both of the controllers are designed based on vector control. The transmission system adopts VSC-HVDC technology. Offshore converter is used to impose a reference grid with constant frequency and voltage magnitude. The onshore converter is controlled to regulate the dc voltage. When an onshore grid fault occurs, it can also provide reactive current to support the restoration of ac voltage. Its controller is designed based on vector control, but another feed-forward term is added to the controller to provide reactive power compensation.

After the controllers are developed for wind turbines and HVDC converters. A test system comprising of OWFs with VSC-HVDC connection to onshore grid has been implemented. It was tested under different wind conditions to verify the steady state condition and afterwards to investigate fault sceneries.

Different types of FRT methods have been tested with the developed system through PSCAD simulation. There are communication based FRT methods, e.g. power set-point adjustment method and active current control method. These two methods reduce the power output from wind turbines by sending a power reduction factor

from HVDC converter to each wind turbine. Their performance largely depends on the communication reliability and communication speed between VSC-HVDC and wind turbines. There are also communication-less FRT methods, e.g. offshore voltage reduction method and chopper resistor method. These two methods do not rely on the communication between VSC-HVDC and wind turbines. The former method blocks the OWF output power by reducing the offshore grid voltage magnitude. It can provide fast power reduction, but because the wind turbines still produce active power, this unbalanced power will accumulate on the wind turbine drive train. As a result, wind turbine drive train will suffer from electrical stress. Chopper resistor method is an quite effective method of controlling the dc voltage within safety level, but a large chopper resistor is quite expensive. The proposal in this thesis is to use an enhanced FRT method, which combines power setpoint method and offshore voltage reduction method, but communication delay is eliminated and the electrical stress on wind turbine train is reduced. The method can be described as follows: when an onshore fault occurs, the offshore converter detects the increase of dc voltage in the HVDC-link and immediately reduces the magnitude of offshore ac voltage. This results in less power transmitted to offshore converter. The power produced by wind turbine generator is also reduced by adding a power reduction factor to GSC. But this power reduction factor is not sent from HVDC converter, it is generated by the wind turbine itself by comparing the reduced offshore ac voltage magnitude and rated offshore ac voltage magnitude. Therefore, there is almost no delay of reducing the wind turbine output power. As a result, the HVDC-link over voltage control ability is largely improved and it can be controlled within its safety limit. Besides, there is also less electrical stress on the wind turbine drive train.

6.2 Future Work

FRT is a quite important issue when large OWFs are connected to main grid. Many grid codes have regulation on it. Therefore an extensive research is still required to design different new methods to meet the FRT requirement from grid codes. The following section contains some suggestions for future work.

- Laboratory experiment could verify and support the effectiveness of the proposed FRT methods.
- Energy storage system, e.g. flywheel and pumped storage can be used to improve the FRT ability of the VSC-HVDC system. This research is outside the scope of this thesis; however, it may be interesting for future studies.
- Recently, Modular multi-level converter (MMC) has become a quite common type of VSC for HVDC. This converter has a better dynamic performance compared to two-level converter. How does it respond to ac grid fault? And how does it contribute to FRT? These questions are interesting to answer.

- Multiterminal DC (MTDC) grid is regarded as an alternative solution to point to point connection, providing high flexibility. The FRT methods in MTDC system need some research.

References

[1] "Global wind energy council." http://www.gwec.net/global-figures/graphs/, 2015.

[2] "The European offshore wind industry-key trends and statistics 2009," tech. rep., EWEA, 2010.

[3] O. A.-L. Anastasios Oulis Rousis, "Dc voltage control for fault management in hvdc system," *12th Deep Sea Offshore Wind R&D Conference*, 2015.

[4] "Wind in power 2014 european statistics," tech. rep., EWEA, 2015.

[5] "Pure power wind energy targets for 2020 and 2030," tech. rep., EWEA, 2011.

[6] C. Ismunandar, "Control of multi-terminal vsc-hvdc for offshore wind power integration," 2010.

[7] T. M. Haileselassie, "Control, dynamics and operation of multi-terminal vsc-hvdc transmission systems," 2012.

[8] M. Bahrman and B. Johnson, "The abcs of hvdc transmission technologies," *Power and Energy Magazine, IEEE*, vol. 5, pp. 32–44, March 2007.

[9] Wikipedia, "Hvdc converter." https://en.wikipedia.org/wiki/HVDC_converter.

[10] P. Haugland, "Its time to connect: Technical description of hvdc light® technology," *ABB Techincal Report*, 2008.

[11] E. Acha, V. Agelidis, O. Anaya, and T. Miller, *Power electronic control in electrical systems*. Elsevier, 2001.

[12] A. R. Årdal, "Feasibility studies on integrating offshore wind power with oil platforms," 2011.

[13] R. E. T. Olguin, "Grid integration of offshore wind farms using hybrid hvdc transmission: Control and operational characteristics," 2013.

[14] J. Machowski, J. Bialek, and J. Bumby, *Power system dynamics: stability and control*. John Wiley & Sons, 2011.

[15] N. Mohan, "Advanced electric drives,"

[16] C. Bajracharya, "Control of vsc-hvdc for wind power," 2008.

[17] L. Xu and B. R. Andersen, "Grid connection of large offshore wind farms using hvdc," *Wind Energy*, vol. 9, no. 4, pp. 371–382, 2006.

[18] S. I. Nanou, G. N. Patsakis, and S. A. Papathanassiou, "Assessment of communication-independent grid code compatibility solutions for vsc–hvdc connected offshore wind farms," *Electric Power Systems Research*, vol. 121, pp. 38–51, 2015.

[19] S. Dash *et al.*, "Modeling and fault analysis of wind turbine with a permanent magnet synchronous generator using pscad," in *International Journal of Engineering Research and Technology*, vol. 3, ESRSA Publications, 2014.

[20] A. Perdana, *Dynamic Models of Wind Turbines*. PhD thesis, Chalmers University of Technology, 2008.

[21] H. Li and Z. Chen, "Overview of different wind generator systems and their comparisons," *IET Renewable Power Generation*, vol. 2, no. 2, pp. 123–138, 2008.

[22] A. D. Hansen, *Generators and power electronics for wind turbines*. John Wiley and Sons, England, 2005.

[23] M. O. Hansen, *Aerodynamics of Wind Turbines*. Routledge, 2013.

[24] A. D. Hansen and L. H. Hansen, "Wind turbine concept market penetration over 10 years (1995–2004)," *Wind energy*, vol. 10, no. 1, pp. 81–97, 2007.

[25] L. H. Hansen, L. Helle, F. Blaabjerg, E. Ritchie, S. Munk-Nielsen, H. W. Bindner, P. E. Sørensen, and B. Bak-Jensen, *Conceptual survey of generators and power electronics for wind turbines*. 2002.

[26] J. Zhang, M. Cheng, Z. Chen, and X. Fu, "Pitch angle control for variable speed wind turbines," in *Electric Utility Deregulation and Restructuring and Power Technologies, 2008. DRPT 2008. Third International Conference on*, pp. 2691–2696, April 2008.

[27] M. Chinchilla, S. Arnaltes, and J. C. Burgos, "Control of permanent-magnet generators applied to variable-speed wind-energy systems connected to the grid," *Energy Conversion, IEEE Transactions on*, vol. 21, no. 1, pp. 130–135, 2006.

[28] S. K. Chaudhary, *Control and Protection of Wind Power Plants with VSC-HVDC Connection*. PhD thesis, Aalborg University, Aalborg, Denmark, 2011.

[29] O. Anaya-Lara, *Offshore wind farm electrical sys.*

[30] C. C. Davidson and D. Trainer, "Innovative concepts for hybrid multi-level converters for hvdc power transmission," in *AC and DC Power Transmission, 2010. ACDC. 9th IET International Conference on*, pp. 1–5, IET, 2010.

[31] S. Maruyama, N. Ishii, M. Shimada, S. Kojima, H. Tanaka, M. Asano, T. Yamanaka, and S. Kawakami, "Development of a 500-kv dc xlpe cable system," *Furukawa review*, vol. 25, pp. 47–52, 2004.

[32] N. Watson and J. Arrillaga, *Power systems electromagnetic transients simulation*. No. 39, Iet, 2003.

[33] HVDC Research Centre, Canada, *PSCAD users Guide*, 2005.

[34] M. Tsili and S. Papathanassiou, "A review of grid code technical requirements for wind farms," *IET Renewable Power Generation*, vol. 3, no. 3, pp. 308–332, 2009.

[35] B. E.ON Netz GmbH, *Grid code high voltage and extra high voltage*. 2006.

[36] O. Anaya-Lara, N. Jenkins, J. Ekanayake, P. Cartwright, and M. Hughes, *Wind energy generation: modelling and control*. John Wiley & Sons, 2011.

[37] G. Ramtharan, A. Arulampalam, J. B. Ekanayake, F. Hughes, and N. Jenkins, "Fault ride through of fully rated converter wind turbines with ac and dc transmission systems," *IET Renewable Power Generation*, vol. 3, no. 4, pp. 426–438, 2009.

[38] C. Feltes, H. Wrede, F. W. Koch, and I. Erlich, "Enhanced fault ride-through method for wind farms connected to the grid through vsc-based hvdc transmission," *Power Systems, IEEE Transactions on*, vol. 24, no. 3, pp. 1537–1546, 2009.

[39] B. Silva, C. Moreira, H. Leite, J. Lopes, *et al.*, "Control strategies for ac fault ride through in multiterminal hvdc grids," *Power Delivery, IEEE Transactions on*, vol. 29, no. 1, pp. 395–405, 2014.

[40] Arulampalam, Ramtharan, Caliao, Ekanayake, and Jenkins, "Simulated onshore-fault ride through of offshore wind farms connected through vsc hvdc," *Wind Engineering*, vol. 32, no. 2, pp. 103–113, 2008.

[41] T. M. Haileselassie, "Control of multi-terminal vsc-hvdc systems," 2008.

[42] P. Anderson and A. Bose, "Stability simulation of wind turbine systems," *Power Apparatus and Systems, IEEE Transactions on*, vol. PAS-102, pp. 3791–3795, Dec 1983.

[43] J. Slootweg, S. de Haan, H. Polinder, and W. Kling, "General model for representing variable speed wind turbines in power system dynamics simulations," *Power Systems, IEEE Transactions on*, vol. 18, pp. 144–151, Feb 2003.

Appendix A

Park Transformation

Park transformation transforms a three phase voltage (current) to the two phase component in the synchronously rotating reference system. It is used in model of VSC and design of VSC controller in this thesis.

Park Transform is given by [41] :

$$\begin{bmatrix} V_d \\ V_q \\ 0 \end{bmatrix} = \frac{2}{3} \begin{bmatrix} \cos\theta & \cos(\theta - \frac{2\pi}{3}) & \cos(\theta + \frac{2\pi}{3}) \\ -\sin\theta & -\sin(\theta - \frac{2\pi}{3}) & -\sin(\theta + \frac{2\pi}{3}) \\ \frac{1}{2} & \frac{1}{2} & \frac{1}{2} \end{bmatrix} \begin{bmatrix} V_a \\ V_b \\ V_c \end{bmatrix}$$

Inverse Park Transform is [41] :

$$\begin{bmatrix} V_a \\ V_b \\ V_c \end{bmatrix} = \frac{2}{3} \begin{bmatrix} \cos\theta & -\sin\theta & 1 \\ \cos(\theta - \frac{2\pi}{3}) & -\sin(\theta - \frac{2\pi}{3}) & 1 \\ \cos(\theta + \frac{2\pi}{3}) & -\sin(\theta + \frac{2\pi}{3}) & 1 \end{bmatrix} \begin{bmatrix} V_d \\ V_q \\ 0 \end{bmatrix}$$

Appendix B

PMSG parameters

PMSG parameters for wind farm 1:

Parameters	value	Unit
Rated power	300	MW
Rated voltage	0.69	kV
Base frequency	50	Hz
d_{axis} reactance X_d	0.5	pu
q_{axis} reactance X_q	0.51	pu
Inertial constant	3	s

Table B.1: *PMSG1 parameters*

PMSG parameters for wind farm 2:

Parameters	value	Unit
Rated power	200	MW
Rated voltage	0.69	kV
Base frequency	50	Hz
d_{axis} reactance X_d	0.45	pu
q_{axis} reactance X_q	0.47	pu
Inertial constant	3	s

Table B.2: *PMSG2 parameters*

Appendix C

Wind Profile

The wind behavior model chosen for this thesis is a four-component model, defined by the equation:

$$V_w = V_m + V_r + V_g + V_n \tag{C.1}$$

where,

V_w is the wind profile.

V_m is the mean wind speed at reference height. It is the base wind velocity.

V_r is ramp wind component. It is a gradual increase of wind speed.

V_g is gust wind component. It is a sudden change of wind speed.

V_n is noise wind component. It is used to specify the random fluctuation of the wind speed.

Refer to [13], [42], and [43] for more information.

C.1 Wind Profile for Wind Farm 1

Mean wind speed at reference height V_m is 10m/s.

Ramp wind component V_r is shown in the following table C.1:

Parameters	value
Ramp maximum velocity	4m/s
Ramp period	30s
Ramp start time	10s

Table C.1: *Ramp wind component for wind farm 1*

Gust wind component V_g is shown in the following table C.2:

Parameters	value
Gust peak velocity	-3m/s
Gust period	10s
Gust start time	15s

Table C.2: *Gust wind component for wind farm 1*

Noise wind component V_n is shown in the following table C.3:

Parameters	value
Number of noise component	150
Surface drag coefficient	0.0192
Turbulence scale	600m
Radom seed number	50
The interval for random generation	0.35

Table C.3: *Noise wind component for wind farm 1*

C.2 Wind Profile for Wind Farm 2

Mean wind speed at reference height V_m is 10m/s. No ramp wind component and gust wind component.

Noise wind component V_n is shown in the following table C.4:

Parameters	value
Number of noise component	50
Surface drag coefficient	0.0192
Turbulence scale	600m
Radom seed number	30
The interval for random generation	0.35

Table C.4: *Noise wind component for wind farm 2*

Appendix D

Control Block of HVDC System

The control system of VSC-HVDC is composed of inner loop control and outer loop control. Based on the basic relationship of the system model, the control block of inner loop can be developed as:

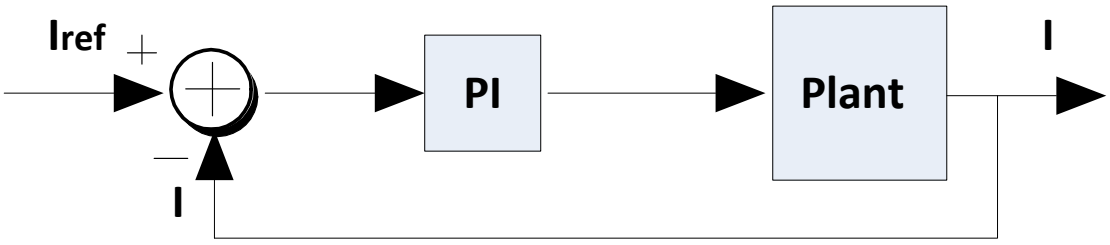

Figure D.1: *Inner current loop*

The inner loop control block mainly consists of PI regulator and plant which represents the system transfer function. The representative equation of the PI regulator is:

$$R(s1) = \frac{K_1(1 + sT_1)}{sT_1} \tag{D.1}$$

where K_1 and T_1 are the parameters of PI controller.

The equation for the plant is:

$$G(s) = \frac{1}{R_{pr}}(\frac{1}{1 + s\frac{L_{pr}}{R_{pr}}}) \tag{D.2}$$

where R_{pr} and L_{pr} represent the resistance and inductance coupling the converter and the grid.

Generally there are four control modes for outer loop controller: dc voltage control, ac voltage control, active power control, and reactive power control. The outer loop controller shown here is based on dc voltage control. The control block for dc voltage is represented by:

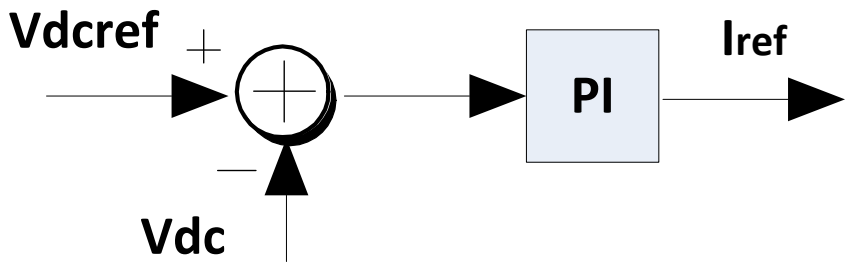

Figure D.2: *Outer dc loop*

The representative equation of the PI regulator is:

$$R(s2) = \frac{K_2(1 + sT_2)}{sT_2} \tag{D.3}$$

where K_2 and T_2 is the parameters of PI controller.

The math relationship between V_{dc} and i_d can be described with the following equation:

$$V_{dc} = \frac{3}{2} i_d v_d \frac{1}{sCV_{DC}} \tag{D.4}$$

where V_{dc} is the instantaneous dc voltage of the dc-link, C is the capacitance of the dc link, v_d is the d component of ac voltage, i_d is the d component of ac current, V_{DC} is the rated dc voltage of the dc-link.

For detailed information, refer to [16]

The overall block for dc control is shown in the following Figure:

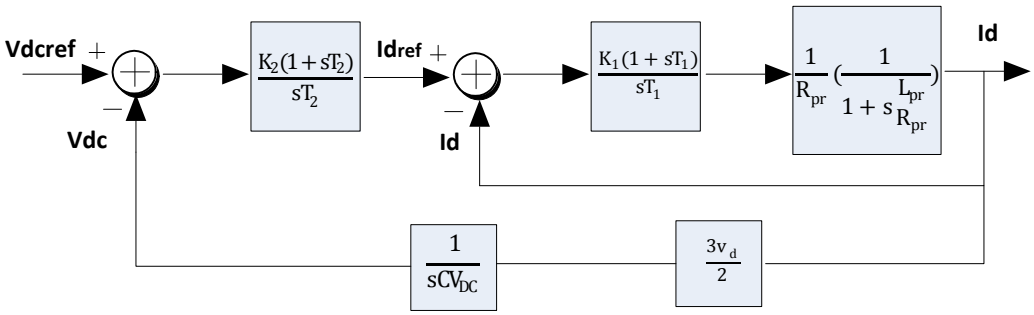

Figure D.3: *Overall PI control loop*

Appendix E

Tuning of PI Controller

Tuning of PI controller includes inner current controller, dc voltage controller, reactive power controller, ac voltage controller, and wind turbine back-to-back controller. The tuning method is based on [28].

E.1 Inner Current Controller

In Figure, R_{pr}=0.5Ω, and L_{pr}=0.051 H Then,

$$\tau = \frac{L_{pr}}{R_{pr}} = 0.102 \tag{E.1}$$

Make T_1=τ=0.102, the open loop poles get canceled, the remaining open loop transfer function is:

$$G_{o1}(s) = \frac{K_1}{sR_{pr}T_1} \tag{E.2}$$

Then the closed loop transfer function is:

$$G_{c1}(s) = \frac{1}{1 + s(\frac{R_{pr}T_1}{K_1})} \tag{E.3}$$

Switch frequency is 2000 Hz, the bandwidth is selected as 390 Hz (or 780rad/s), then

$$\frac{1}{1 + s(\frac{R_{pr}T_1}{K_1})} = \frac{1}{1 + \frac{s}{780\pi}} \tag{E.4}$$

From the equation above, the value of K_1 can be calculated:

$$K_1 = 780\pi R_{pr} T_1 = 124.9 \tag{E.5}$$

E.2 Outer DC Voltage Controller

After pole cancellation, the inner loop transfer function becomes:

$$G_{in}(s) = \frac{1}{1 + \frac{s}{780\pi}} \tag{E.6}$$

Pole cnacellation for outer loop is achieved, when:

$$T_2 = \frac{1}{780\pi} = 0.00041 \tag{E.7}$$

For the outer loop, the integral function $\frac{1}{s}$ is replaced by Δt, which implies multiplication by the time period. In this thesis, Δt=$\frac{1}{2000}$. Then the open loop transfer function becomes:

$$G_{o2}(s) = \frac{K_2}{sT_2} \frac{3v_d \Delta t}{2CV_{DC}} \tag{E.8}$$

The closed loop transfer function is:

$$G_{c2}(s) = \frac{1}{1 + \frac{2sCV_{DC}T_2}{3v_d K_2 \Delta t}} \tag{E.9}$$

Bandwidth is selected at 19.5 Hz or 39π, then:

$$\frac{2sCV_{DC}T_2}{3v_d K_2 \Delta t} = \frac{1}{39\pi} \tag{E.10}$$

K_2 can be calculated by:

$$K_2 = 39\pi \frac{2CV_{DC}T_2}{3v_d \Delta t} = 0.00357 \tag{E.11}$$

E.3 Outer Reactive Power Controller and AC voltage controller

The relationship between reactive power and q component of ac current is shown in the following equation:

$$Q = -\frac{3}{2} v_d i_q \tag{E.12}$$

Then the open loop transfer function for reactive power is:

$$G_{o3}(s) = \frac{K_3}{sT_2} \frac{3v_d}{2} \tag{E.13}$$

The closed loop transfer function becomes:

$$G_{c3}(s) = \frac{1}{1 + \frac{2sT_2}{3v_d K_3}} \tag{E.14}$$

Bandwidth is selected at 39 Hz or 78π, then:

$$K_3 = 78\pi \frac{2T_2}{3v_d} = 0.000357 \tag{E.15}$$

AC voltage controller is chosen via trail and error to get a reasonable speed of response and slower than the inner current controller.

E.4 Wind Turbine back-to-back Converter Controller

The dc voltage controller, reactive power controller, and inner current controller is tuned based on the same principle of VSC-HVDC controller.

Since active power control and reactive power control has very similar transfer function, the active power controller of the generator side controller is tuned following the rule of tuning reactive power controller.